

## Single-molecule live cell imaging of the Smc5/6 DNA repair complex

Thomas J. Etheridge<sup>1\*</sup>, Desiree Villahermosa<sup>1</sup>, Anja Irmisch<sup>1,3</sup>, Adam T. Watson<sup>1</sup>, Alex Herbert<sup>1</sup>, Hung Q. Dang<sup>1,4</sup>, Mark A. Osborne<sup>2</sup>, Antony W. Oliver<sup>1</sup>, Antony M. Carr<sup>1</sup> and Johanne M. Murray<sup>1\*</sup>

<sup>1</sup> Genome Damage and Stability Centre, School of Life Sciences, University of Sussex, Falmer, UK.

<sup>2</sup> Chemistry Department, School of Life Sciences, University of Sussex, Falmer, UK.

<sup>3</sup> Current address: Department of Dermatology, University Hospital Zürich, Switzerland.

<sup>4</sup> Current address: Texas A&M University, Texas, United States.

\*Correspondence:

[j.m.murray@sussex.ac.uk](mailto:j.m.murray@sussex.ac.uk), [t.etheridge@sussex.ac.uk](mailto:t.etheridge@sussex.ac.uk),

### Abstract

The Smc5/6 complex is involved in various DNA transactions and is best known for ensuring the fidelity of homologous recombination. We exploit single-molecule tracking in live fission yeast to investigate Smc5/6 chromatin association. We show that Smc5/6 is chromatin associated in unchallenged cells and this depends on the non-SMC protein Nse6. We define a minimum of two Nse6-dependent sub-pathways, one of which requires the BRCT-domain protein Brc1. Using defined mutants in genes encoding the core Smc5/6 complex subunits we show that the Nse3 double-stranded DNA binding activity and the two arginine fingers of the two Smc5/6 ATPase binding sites are critical for chromatin association. Interestingly, disrupting the ssDNA binding activity at the hinge region does not prevent chromatin association. However, unlike a mutant attenuating chromatin association, a mutant that disrupts ssDNA binding results in highly elevated levels of gross chromosomal rearrangements during replication restart. This is consistent with a downstream function for ssDNA binding in regulating homologous recombination.

## Introduction

The structural maintenance of chromosomes (SMC) complexes cohesin, condensin and Smc5/6 are critical for the correct organisation of chromosome architecture<sup>1</sup>. Whereas the functions of cohesin and condensin are increasingly well understood, the Smc5/6 complex remains relatively ambiguous. Smc5/6 is conserved across all eukaryotes and is best known for its role in the cellular response to DNA damage by ensuring the fidelity of homologous recombination repair (HRR)<sup>2,3</sup>. Smc5/6 has been reported to promote replication fork stability<sup>4</sup> and facilitate DNA replication through natural pausing sites<sup>5</sup>. Biochemically, the complex can regulate pro-recombinogenic helicases<sup>6,7</sup>. It has also been proposed to monitor DNA topology<sup>8</sup> and recently been shown to restrict viral transcription<sup>9,10</sup>. Complete inactivation of the Smc5/6 complex in a variety of organisms leads to cell death. However, hypomorphic mutants show significant defects in sister-chromatid HRR, display replication fork instability, are sensitive to a wide range of genotoxins and accumulate unresolved recombination intermediates<sup>4,11,12</sup>.

Like all SMC complexes, the core of Smc5/6 is composed of two folded proteins, Smc5 and Smc6, which form a heterodimer (Figure 1A). Each subunit comprises a long coiled-coil arm with a hinge region at one end and a globular ATPase head at the other<sup>1</sup>. All three SMC heterodimers interact at the hinge and ATP binding/hydrolysis occurs in two pockets formed between the heads of the two subunits. For all SMC complexes, ATP turnover is essential for cell viability and has been proposed to bring about conformational changes in the arms<sup>13,14,15</sup>. The ATPase activity is also key to the interaction of SMC's with DNA: Cohesin's ATPase is required for both loading and dissociation from DNA<sup>16</sup>, whilst condensin is dependent on its ATPase activity for translocating along DNA and forming loop structures<sup>17,18</sup>. The role of the Smc5/6 ATPase in DNA association has not been studied in detail.

The Smc5/6 hinge contains specialised interfaces that are important for interacting with single stranded DNA (ssDNA)<sup>19</sup>. Disruption of these regions by mutation results in sensitivity to DNA damaging agents. The Smc5/6 ATPase heads are bridged by a sub-complex of three non-SMC elements (Nse), Nse4 (kleisin) and two kleisin-interacting tandem winged-helix element (KITE) proteins, Nse1 and Nse3. Nse1 has a RING finger and, in association with Nse3, has been shown to have ubiquitin ligase activity<sup>20</sup>. The winged-helix domain of Nse3 possesses double-stranded DNA (dsDNA) binding activity, which is essential for viability<sup>21</sup>. The dsDNA

binding has been predicted to provide the basis for initial chromatin association and loading of the complex<sup>21</sup>. In addition to the Nse1,3,4 subcomplex, Nse2, a SUMO ligase, is associated with the Smc5 coiled-coil arm. DNA association of the Smc5/6 complex is required to activate the Nse2 SUMO ligase, which SUMOylates a range of targets within and outside of the complex<sup>22</sup>. Two further proteins, Nse5 and Nse6, also associate, albeit not stoichiometrically, with the Smc5/6 complex in yeasts (both *S. cerevisiae* and *S. pombe*). However, unlike the other Nse proteins, Nse5 and Nse6 have not been identified as part of a Smc5/6 holo-complex in human cells<sup>23,24</sup>.

Chromatin loading of the structurally related cohesin complex requires accessory proteins, the cohesin-loader complex Scc2–Scc4 (*sp*Mis4–Ssl3)<sup>25</sup>. A loading complex for Smc5/6 has not yet been defined but recent work in fission yeast has shown that its recruitment to sites of replication fork collapse occurs via a multi-BRCT domain protein, Brc1<sup>26</sup>. Brc1 binds to  $\gamma$ -H2A and interacts with the Nse5-Nse6 subcomplex (which associates with Smc5/6 but is not part of the core complex), providing a potential mechanism by which Smc5/6 is recruited and loaded. In *S. cerevisiae* the N-terminal four BRCT domains of the Brc1 homologue, Rtt107, have also been shown to bind Nse6 amongst a number of other proteins in the DNA damage response<sup>27</sup>. In human cells recruitment of Smc5/6 to inter-strand cross-links was shown to depend on interactions between SLF1, another multi-BRCT domain protein, and SLF2 - a distant homologue of Nse6<sup>28</sup>. These observations suggest that recruitment of Smc5/6 through Nse6 and a BRCT-domain mediator protein has been conserved through evolution.

Understanding how Smc5/6 associates with chromatin is an important step in defining how it regulates recombination processes and other potential DNA transactions. To date, the study of Smc5/6 chromatin association has been mostly limited to chromatin immunoprecipitation (ChIP)-based methodologies. Genome-wide studies have demonstrated that, in unperturbed cells, Smc5/6 accumulates at regions containing highly repetitive DNA such as telomeres, centromeres and the ribosomal DNA (rDNA) array<sup>29,30</sup>. Enrichment of the complex at these discrete genomic loci has been reported in cells treated with exogenous genotoxic agents such as methane methylsulfonate (MMS) and hydroxyurea (HU)<sup>29</sup>. Smc5/6 localisation has also been reported to frequently coincide with cohesin binding sites<sup>8</sup>.

Here, we set out to monitor the dynamic behaviour of Smc5/6 in live fission yeast cells using photoactivated localisation microscopy (PALM) to investigate the role of its ATPase activity, DNA binding sites and protein binding partners in promoting chromatin association. By comparing Smc5/6 with condensin and cohesin we validate our approach by demonstrating that the three complexes display distinct chromatin association dynamics and spatial distribution in cycling cells. By deleting key interacting partners of the core Smc5/6 complex, we establish that Nse5-Nse6 is required for almost all chromatin association, whereas Brc1 is required for only a proportion of the association. These data define the Brc1-Nse6-dependent sub-pathway of chromatin loading and identify parallel Nse6-dependent but Brc1-independent sub-pathway(s). We next analysed the chromatin-associated fraction of the Smc5/6 complex in a range of *smc* and *nse* mutant backgrounds. This highlighted that ATPase activity and dsDNA binding are both crucial for chromatin association, whereas ssDNA binding at the hinge is dispensable. Additionally, we show that a mutant defective in ssDNA binding, in contrast to a mutant defective in chromatin association, has a strong defect in suppressing non-allelic homologous recombination in response to replication fork arrest.

## Results

### *Single-particle tracking PALM of SMC proteins in fission yeast*

To monitor SMC complexes in living yeast cells we employed single-particle tracking photoactivated localisation microscopy (sptPALM)<sup>31</sup>. With this method the chromatin association status of individual molecules can be inferred by measurement of their apparent diffusivities: DNA-bound proteins have substantially constrained diffusion compared to those that are freely diffusing<sup>32</sup>. We created fission yeast strains that endogenously expressed the kleisin subunits of Smc5/6 (Nse4), cohesin (Rad21) and condensin (Cnd2) fused to the photoconvertible fluorophore mEos3 (Figure 1A and 1B). Tagging kleisin subunits has been a widely adopted means of monitoring SMC complexes via ChIP or microscopy and our mEos3-tagged alleles had no measurable impact on cellular proliferation (Figure S1A).

In *S. pombe* the condensin kleisin, Cnd2, resides in the cytoplasm during interphase and is imported into the nucleus at the onset of mitosis<sup>33</sup>. We used this phenomenon to assess the ability of sptPALM to detect and evaluate the chromatin association of SMC proteins. To

visualise single mEos3-labelled condensin complexes, we stochastically photoconverted the mEos3 fluorophore using pulses of 405nm light and imaged using near-TIRF excitation beam and a 20ms camera exposure time. Single molecules were localised and tracked using custom-written software (see *Materials and Methods*). Cumulative localisation images of Cnd2-mEos3 showed nuclear import in a subset of cells, whereas the rest of the cells in the population showed only cytoplasmic localisation, concurrent with previous observations (Figure 1C).

We employed the recently published ‘Spot-On’ software to interpret and analyse the Cnd2-mEos3 single-molecule tracking data<sup>34</sup>. Spot-On is a bias-aware software package that extracts kinetic parameters from histograms of single molecule displacements (or ‘jump distances’) over time and extrapolates fractions of different sub-populations of molecules (e.g. bound, free). We isolated single-molecule tracks from interphase cells with no clear nuclear Cnd2 and those from mitotic cells. Displacement histograms derived from the two data sets show clear differences in the diffusivity of Cnd2, with mitotic cells displaying a large population of shorter displacements equating to chromatin bound complexes (Figure 1D). Fitting of a Spot-On model to this data revealed a substantial increase in the fraction of molecules in mitotic cells that were chromatin bound (Figure 1E). These data demonstrate that sptPALM is an effective method to monitor chromatin association of SMC complexes in live cells.

#### *Smc5/6 chromatin association is also distinct from cohesin*

We next examined the chromatin association of cohesin and Smc5/6 using our sptPALM workflow. Asynchronously growing cells expressing either Rad21-mEos3 or Nse4-mEos3 were imaged and processed similarly to Cnd2-mEos3. Displacement histograms revealed distinct profiles for each of the two complexes, with Rad21 (cohesin) displaying a much higher proportion of short displacements (Figure 2A). This was reflected in the Spot-On modelling which showed the fraction of chromatin-bound Rad21 was significantly higher than Nse4 (Figure 2B, S1B). The difference in behaviour was confirmed when other subunits of cohesin (Smc1) and Smc5/6 (Nse2, Smc6) were tagged with mEos3. Both cohesin subunits behaved the same, as did the three Smc5/6 subunits, indicating that the dynamics of the whole SMC complex is observed with the labelled kleisin (Figure S1C, D). Cumulative nuclear localisation images highlight the disparity between the two complexes: Rad21-mEos3 localisations are mainly sequestered in nuclear foci indicating high levels of chromatin association (Figure 2C) while Nse4-mEos3 demonstrated a mix of foci and diffuse localisations. This result is

intriguing as the complexes have been found to localise to the same regions of the genome in genome-wide ChIP assays<sup>8,30</sup>. Notably, whilst Rad21 displacement data could be fitted reasonably robustly with a Spot-On 2-state kinetic model, that for Nse4 was significantly better described by a 3-state fit that includes an intermediate "slow-diffusing" population (Figure S2). However, it is not clear whether this third state describes transient interactions with chromatin or arises from anomalous diffusion as a result of a crowded molecular environment<sup>35</sup>. Nonetheless, irrespective of the minor differences seen in the chromatin bound fraction between a 2- or 3-state fit (Figure S2), taken together these observations show that interaction of cohesin and Smc5/6 with chromatin are distinct and different and suggest that their association occurs with different dynamics.

#### *Different requirements for Nse6 and Brc1 for recruitment of Smc5/6*

Recent work in fission yeast has shown that the Nse6 subunit and the BRCT-containing protein Brc1 are required for the recruitment of Smc5/6 to distinct nuclear foci in response to DNA damage<sup>26</sup> (Figure 3A). To investigate how these factors influence recruitment of the Smc5/6 complex to chromatin in unchallenged cells we first tagged Nse6 with mEos3 and compared its behaviour to Nse4 (Figure 3B). In contrast to Nse2 and Smc6, which show similar chromatin association to Nse4 (Figure S1C, D), Nse6 showed a broader range of displacements and was less chromatin associated (Figure 3B). This suggests Nse6 is not always associated with the core Smc5/6 complex, but rather is consistent with Nse6 acting as a loader or stabilizing factor for Smc5/6.

Next, the genes encoding Brc1 and Nse6 were deleted in the Nse4-mEos3 strain and Smc5/6 chromatin association monitored by sptPALM. Deletion of either *brc1* or *nse6* resulted in an altered displacement profile and a concurrent decrease in the fraction of bound molecules (Figure 3C, D). In *brc1*Δ the amount of chromatin associated Smc5/6 decreased by approximately 50% showing that only a proportion of Smc5/6 chromatin association is dependent on Brc1. In contrast, deletion of *nse6* showed significant deviation from the wild type data, resulting in an almost complete loss of chromatin associated Nse4 (Figure 3D). These data strongly support a role for Nse6 as either a Smc5/6 loader or a factor that stabilises Smc5/6 on the chromatin following transient association. It should be emphasised that *nse6* deleted *S. pombe* cells are slow growing and very sensitive to genotoxins, whereas deletion of genes

encoding proteins in the core complex are inviable. This suggests that Smc5/6 can still associate with chromatin in the absence of Nse6, albeit at a much-reduced level.

Using ChIP experiments it has been reported that Smc5/6 is enriched at repetitive genomic loci following MMS treatment and that this is dependent on Brc1 and Nse6<sup>26</sup>. We therefore tested whether we could detect increased Nse4 chromatin association in response to MMS treatment in *brc1+ nse6+*, *brc1Δ* and *nse6Δ* cells. Acute exposure to 0.03% MMS for 5 hours resulted in a modest increase in the fraction of Nse4-mEos3 bound to the chromatin in cells with a wild type background (Figure 3E). However, both *brc1Δ* and *nse6Δ* failed to show any increase above levels detected in untreated cells. These data support the hypothesis that both Brc1 and Nse6 are required for Smc5/6 recruitment to sites of DNA damage<sup>26</sup>. They further show that Nse6 plays a major Brc1-independent role in loading Smc5/6 in the absence of exogenous DNA damage. Brc1 is reported to associate specifically with  $\gamma$ -H2A<sup>36</sup>. We therefore tested Smc5/6 complex recruitment in *hta1-SA hta2-SA* mutant cells<sup>37</sup>. A statistically significant reduction was evident (Figure 3F), consistent with Brc1-dependant loading being largely confined to regions of  $\gamma$ -H2A.

#### *Smc5/6 ATPase activity is required for efficient chromatin association*

Each of the SMC complexes possess ATPase activity, with two separate and distinct active sites within juxtaposed ‘head’ domains, which are generated by bringing together the required signature motifs *in trans* (Figure 4A). Like all SMC complexes the ATPase activity of Smc5/6 is essential and mutations in either of the two Walker motifs are non-viable<sup>38,39</sup>. Therefore, to investigate the influence of ATPase activity on chromatin-association of the Smc5/6 complex, we first mutated the ‘arginine-finger’ of Smc5 (*smc5-R77A*) or Smc6 (*smc6-R150A*). Mutation of the equivalent residues in other SMC complexes does not typically affect the basal level of ATP turnover, but instead acts to abolish stimulation of activity by DNA-interaction<sup>40</sup>. Both the *smc5-R77A* and the *smc6-R150A* mutation resulted in an increased sensitivity to replication stress (Figure S3A). Tracking of Nse4-mEos3 in these genetic backgrounds revealed decreases in chromatin association of the Smc5/6 complex (Figure 4B, S3B). *smc6-R150A* led to a dramatic decrease in chromatin association whereas mutation of the Smc5 arginine was noticeably less detrimental. Interestingly, the reduction in the levels of chromatin association

correlated with sensitivity to exogenous genotoxic agents, strongly suggesting that DNA-dependent ATP hydrolysis by the two binding pockets is not equivalent.

The Smc6 arginine finger mutant was of particular interest to us as the well characterised *smc6-74* allele maps to the next residue, A151T<sup>4,38,34,42</sup>. Single particle tracking showed this mutant to have a similar decrease in chromatin association to *smc6-R150A*. Sequence-threaded homology models for the head domain of *S. pombe* Smc6 and comparison to the X-ray crystal structure of the head domain from *Pyrococcus furiosus* SMC in complex with ATP (PfSMC, PDB: 1XEX) allowed us to create specific mutations designed to display a graduated effect on the Smc6 arginine-finger: Thr135 in Smc6 was mutated to a series of hydrophobic amino acids with increasing size, each predicted to produce increasingly severe steric clashes with the arginine-finger when engaged in interaction with bound ATP (Figure 4C).

Phenotypic analysis of each *smc6* mutant confirmed that the predicted severity of steric clash (Phe>Leu>Val) closely correlated with an increase in sensitivity to a range of genotoxic agents (Figure 4D), culminating with the most severe mutation, T135F, producing a phenotype similar to the well characterised *smc6-74* (A151T) mutant. Single-particle tracking data revealed that increasing the severity of the substitution corresponded with a decrease in the fraction of bound Smc5/6 (Figure 4E, S3C). The *smc6-T135F* strain showed the same levels of bound complex as the *smc6-74* mutation.

Since mutations in the ATPase domains render cells sensitive to replication stress (Figure 4D) we monitored whether these mutants could recruit the complex to chromatin after treatment with MMS. We treated the ATPase mutants with 0.03% MMS over 5 hours and measured the fraction of chromatin bound molecules (Figure S3D). The mutations prevented Smc5/6 from being recruited to chromatin in response to MMS. Together these data demonstrate that the ability to stimulate Smc5/6 ATPase activity through the arginine finger is crucial for its stable association with the chromatin. The disparity in phenotype between *smc6* and *smc5* ATPase mutants suggests there could be an underlying asymmetry in the use for the two ATP binding sites, a phenomenon that has been recently described for both condensin and cohesin<sup>16,43</sup>.

### *ssDNA binding is dispensable for Smc5/6 chromatin association*

Smc5/6 has been shown to bind both ds- and ssDNA at the head and hinge respectively (Figure 5A). The KITE protein Nse3 has a dsDNA binding domain in both humans and fission yeast. This is essential and was predicted to be the initial point of interaction between Smc5/6 and the chromatin required before loading<sup>21</sup>. To assess whether Nse3 dsDNA interaction plays a role in global chromatin association we introduced the hypomorphic allele *nse3-R254E*, known to disrupt (but not abolish) dsDNA binding by Nse3, into the Nse4-mEos3 strain and performed sptPALM. When compared to *nse3*<sup>+</sup>, Nse4-mEos3 displacement histograms from asynchronous *nse4-mEos3 nse3-R254E* cells showed a broader profile which resulted in a reduction in the fraction of bound molecules (Figure 5B). This confirms *in vivo* that dsDNA binding by Nse3 underpins the chromatin association of Smc5/6 and is consistent with DNA-dependent stimulation of the ATPase activity through the arginine finger domains being coupled to loading.

We recently determined the structure of the *S. pombe* Smc5/6 hinge and identified specialised ‘latch’ and ‘hub’ interfaces that interact with ssDNA (Figure 5C). Like mutants compromised for dsDNA binding, mutants defective in ssDNA binding remain viable but are sensitive to replication stress and DNA damaging agents<sup>19</sup>. We therefore tested whether the ability to bind ssDNA affected the ability of Smc5/6 to associate with chromatin. Mutations that affect ssDNA binding at either the Smc5 latch (*smc5-R609E R615E*, *smc5-Y612G*) or the Smc6 hub (*smc6-F528A*, *smc6-X (R706C)*) were introduced into the Nse4-mEos3 strain. sptPALM experiments performed on asynchronously growing cells showed that, unlike the dsDNA binding and ATPase mutants, disruption of ssDNA binding did not alter the fraction of chromatin associated Smc5/6 (Figure 5D). These data show that, while dsDNA binding is required for the association of the Smc5/6 complex onto chromatin, the interactions with ssDNA are not required for chromatin association and likely ssDNA binding plays a role in downstream DNA repair-associated processes.

Since mutations in the ssDNA binding domains of Smc5/6 render cells sensitive to replication stress<sup>19</sup> we monitored whether these mutants could recruit the complex to chromatin after treatment with MMS. ssDNA binding mutants were treated with 0.03% MMS over 5 hours and the fraction of chromatin bound molecules measured (Figure 5E). The mutations either significantly reduced, or prevented, Smc5/6 from being recruited to chromatin in response to

MMS. We speculate that the ssDNA interaction is required to promote retention on the DNA during DNA replication stress, consistent with ssDNA binding playing a role in processes downstream of loading.

### *ssDNA binding is required to prevent gross chromosomal rearrangements*

Our data indicate that the damage-independent Smc5/6 chromatin association requires the ATPase and dsDNA binding activities of the complex, but not the ssDNA binding. This has led us to speculate (see above) that ssDNA binding is particularly important for regulation of DNA repair and acts downstream of chromatin association. To investigate if distinct phenotypes are associated with ssDNA binding mutants when compared to mutants that affect chromatin association, we investigated the effect of a Smc5/6 hinge (ssDNA binding) and a Smc6 ATPase mutation in the response to replication stress.

In fission yeast, binding of Rtf1 to the polar replication termination sequence, *RTS1*, enforces unidirectional replication of the mating type (*MAT*) region by arresting replication forks emanation from the centromere proximal side of the *MAT* locus<sup>44</sup>. In a previously developed system<sup>45</sup>, two copies of *RTS1* were placed in an inverted orientation on either side of the *ura4* marker on chromosome III (Figure 6A: left panel) to form a locus known as *RuraR*. To regulate *RTS1* barrier activity, *rtf1+* is placed under the control of the *nmt41* (no message in thiamine) promoter. Induction of *rtf1+* leads to arrest of replication forks converging on both *RTS1* sequences (Figure 6A: right panel) and requires that replication of the intervening *ura4* region is dependent on homologous recombination-dependent replication restart. In the absence of key HR factors, such as Rad51, induction of arrest leads to viability loss<sup>45</sup>.

Using the *RuraR* system we compared the ATP-hydrolysis mutant *smc6-A151T* (*smc6-74*) to the hinge ssDNA binding mutant *smc6-R706C* (*smc6-X*). Despite the fact that both *smc6-X* (R706C) and *smc6-74* (A151T) are epistatic to *rad51-d* in response to MMS, there was no loss of viability when stalling was induced at *RTS1* in these backgrounds (Figure S4A). This is consistent with Smc5/6 regulating recombination, rather than being core to the recombination process<sup>2</sup>. HR-dependent replication restart increases genome instability by two distinct mechanisms that can be distinguished in the *RuraR* system: (i) non-allelic homologous recombination (NAHR) events at the point of restart that result in large-scale genomic rearrangements<sup>46</sup> and (ii), the error prone nature of the restarted forks leads to small scale errors

such as replication slippage as the non-canonical fork progresses<sup>47</sup>. The loss of *ura4* in the *RuraR* system provides a readout that is particularly useful to characterise NAHR events (Figure S4B).

Induction of replication arrest led to an increase in the loss of *ura4* activity in *smc6+*, *smc6-74* and *smc6-X* backgrounds. There was only a modest change in the ATPase mutant (*smc6-74*), but the hinge mutant (*smc6-X*) showed a highly elevated induction of *ura4* loss, an 11-fold increase over *smc6+* (Figure 6B, S5 and Table S1). Analysis of the *ura4<sup>-</sup>* colonies isolated after replication stalling (Figure S4C) showed that most were full deletions of the intervening sequence between the two *RTSI* loci. These were significantly increased (16-fold) in the hinge mutant, *smc6-X* (Table S2). The uninduced (*nmt1* off) also showed a 4-fold increase over wild type for *smc6-X*. As the *nmt* promoter is slightly leaky, this is consistent with this mutant being particularly sensitive to very low levels of replication stalling. A second readout of NAHR using the *RuraR* system is that a proportion of *ura4<sup>-</sup>* colonies represent ectopic recombination events between *RTSI* sequences on chromosome III and the native *RTSI* at the *MAT* locus on chromosome II. This results in the reciprocal exchange of chromosome arms (translocation). The hinge ssDNA binding mutant (*smc6-X*) showed a higher number of chromosome II/III junction-positive colonies when *RuraR* arrest was induced (6 in 36), a 62-fold increase over *smc6+* (Table S2). Taken together, these results indicate that the ssDNA binding region of the hinge is particularly important for the suppression of NAHR and gross chromosomal rearrangements.

## Discussion

The Smc5/6 complex is defined as a component of the DNA repair machinery that ensures the fidelity of homologous recombination (HR). However, the complex is essential in yeast which suggests it possesses additional functions beyond HR as deletions of core HR factors are viable<sup>3</sup>. The recruitment of Smc5/6 to DNA and ATP binding and hydrolysis at both the ATP sites are thought to be essential for each of its cellular roles. Understanding the molecular details of how Smc5/6 associates with DNA and/or chromatin is therefore an important step in elucidating how Smc5/6 regulates recombination and other potential DNA transactions. Here, we provide the first *in vivo* single-molecule characterisation of the Smc5/6 complex and demonstrate key requirements for its association with chromatin in live fission yeast.

We show that, in *S. pombe*, the spatial distribution and fraction of chromatin-associated Smc5/6 complexes are markedly different from those of condensin and cohesin. Condensin in interphase cells is excluded from the nucleus and enters the nucleus at the onset of mitosis<sup>33</sup>. We observed that cytoplasmic condensin is freely diffusing, while mitotic nuclear condensin is >50% chromatin associated and thus shows constrained diffusion. This validates our assay. Smc5/6, like cohesin, is primarily nuclear localised throughout the cell cycle. We observed that a significantly larger proportion of Smc5/6 complexes are freely diffusing in the nucleus when compared to cohesin (60% v 20%). This shows that the chromatin association cycles of Smc5/6 and cohesin occur with very different dynamics: Smc5/6 may associate more transiently with chromatin upon recruitment to specific DNA structures. As these complexes have been reported to accumulate at similar genomic loci in genome-wide studies<sup>8</sup>, these observations are important to consider when speculating about interplay between the two complexes.

### *Smc5/6 complex features that influence chromatin association*

The Smc5/6 complex contains two separate ATP binding and hydrolysis sites. Both are formed when the Smc5 and Smc6 head domains interact. In common with all SMC complexes, the ATP binding pockets have an arginine finger domain that is proposed to regulate DNA-dependent ATP hydrolysis. One of the original *smc6* mutants, *smc6-74* (A151T) maps to the residue adjacent to the arginine residue in the arginine finger domain, suggesting it is compromised in ATP hydrolysis. Using a structural model based on the *Pyrococcus furiosus* SMC head domain, we engineered a series of structurally informed mutations designed to compromise the arginine finger to various degrees. Indeed, this allowed us to "dial in"

sensitivity to DNA damaging agents that robustly correlated with a reduced ability of Smc5/6 to associate with chromatin. This strongly suggest that ATPase activity stimulated by DNA binding is pre-requisite for Smc5/6 complex DNA/chromatin association and function. Interestingly, we also uncovered an underlying asymmetry in the requirement for the two ATP binding sites of Smc5 and Smc6. This asymmetry is in line with observations made for cohesin and condensin<sup>18,43</sup> and may signify a downstream role for the Smc5 ATP binding site during HR.

Recent structural and biophysical data for the ssDNA-binding activity of the Smc5/6 hinge domain<sup>19</sup> and the dsDNA-binding Nse1/3/4 module<sup>21</sup> allowed an investigation of the role for each of these two functions in promoting Smc5/6 chromatin association. The introduction of defined mutations into fission yeast demonstrated that dsDNA-binding by Nse3 is required for DNA/chromatin association of the Smc5/6 complex, whereas the ability to bind ssDNA at the hinge is dispensable. Since ssDNA-binding mutants are sensitive to a range of genotoxic agents<sup>19</sup>, we therefore predicted that ssDNA binding most likely plays a role in downstream processes once the complex has initially bound to dsDNA/chromatin. This would be an analogous situation to cohesin whereby after initial DNA binding to dsDNA, capture of a second DNA moiety is only achievable for ssDNA<sup>48</sup>. This prediction is supported by results from our site-specific stall experiments, which indicate that ectopic recombination occurs in Smc5/6 mutants that lack the ability to interact with ssDNA correctly. This does not occur in mutants that fail to stimulate ATPase activity and do not correctly associate with chromatin.

#### *Interacting factors influencing Smc5/6 chromatin association*

Both Brc1 and Nse6 have been implicated in recruiting Smc5/6 to regions of  $\gamma$ -H2A at stalled/collapsed replication forks<sup>26</sup>. We demonstrate here that deletion of either one of these factors reduces the *in vivo* levels of chromatin-associated Smc5/6, in both unchallenged cells and after exposure to MMS. Interestingly, deletion of *brc1* or preventing histone H2A phosphorylation did not generate as severe a defect in chromatin association as deletion of *nse6*. This is in agreement with recent ChIP experiments performed at discreet genomic loci<sup>26</sup>. This demonstrates that there is at least one alternative Brc1-independent pathway for recruitment of Smc5/6 to chromatin. We consider two models that are not mutually exclusive to explain the data. The first model is that the Nse5/6 heterodimer acts directly as a loader of Smc5/6, much like the model for Mis4-Ssl3 being the loader for cohesin<sup>25,49</sup>. In this model

loading would occur via the Nse5/6 subcomplex bridging between Smc5/6 and chromatin associated factors, including Brc1 and other as yet unknown interacting partner(s). This would serve to recruit the Smc5/6 complex to sites with specific features, such as  $\gamma$ -H2A. In this way, indirect recruitment of Smc5/6 via different Nse5/6-interacting partners would serve to bring the complex to specific DNA structures, including collapsed replication forks, HR intermediates and double strand breaks.

The second model proposes that Smc5/6 has an intrinsic ability to associate with DNA, and therefore chromatin, through the dsDNA binding site of Nse3. Nse5-Nse6 has inherent affinity for the complex and, when associated, acts transiently to stabilise the interaction between the Smc5/6 complex and chromatin. In this scenario, other Nse5-Nse6 interacting partners (such as Brc1) act to recruit Nse5-Nse6 to sites with specific features. This serves to enhance the potential for interaction between Nse5/Nse6 and Smc5/6, stabilising the Smc5/6 complex on the chromatin at the sites where it is required. This model would help explain the important observation that, while Smc5, Smc6 and Nse1-4 are all essential proteins, fission yeast cells can survive without Nse5 and Nse6: the Smc5/6 complex can still associate with DNA in the absence of the "loader", but is only inefficiently stabilised on the DNA in the absence of Nse5/6. Furthermore, if a transient association of Nse5/6 with Smc5/6 were required to stabilise DNA/chromatin association after an initial recruitment by dsDNA binding, this would explain both the essential nature of the dsDNA binding activity of Nse3 and the observations that dsDNA binding site is tightly linked to chromatin association.

By conducting a detailed characterisation of Smc5/6 chromatin association in live cells we demonstrate that sptPALM is a powerful approach for studying chromatin associated processes. This methodology, when coupled with structure-led mutational analysis and other techniques, has provided new insights into Smc5/6 behaviour as well as clarifying previous observations from past genetic and molecular genetic experiments. It will be interesting to use this approach in the future to compare the behaviour, association kinetics and residency times of Smc5/6 and cohesin in budding and fission yeast and in human cells as this will inform our understanding of how Smc5/6 functions to regulate homologous recombination and the response to replication stress.

## Materials and Methods

### *S. pombe* strain construction

*S. pombe* strains were constructed using Cre-lox mediated cassette exchange (RMCE) as previously described<sup>50</sup>. Strains were created either with essential gene replacement base strains or C-terminal tagging base strains (Supplementary table 3). C-terminal base strains were transformed with plasmid pAW8-mEos3.2-KanMX6 to introduce the mEos3.2 tag at the C-terminal end of the gene.

### *Microscopy sample preparation*

*S. pombe* cultures were grown to mid-log phase at 30°C in Edinburgh minimal media (EMM) supplemented with leucine, uracil and adenine. Cells were harvested and washed once in phosphate buffered saline (PBS). Cells were then resuspended in PBS and 10µl was deposited on an EMM-agarose pad before being mounted on ozone-cleaned circular coverslips (Thorlabs, #1.5H, Ø25mm) and placed in a metal cell chamber for imaging (Attofluor, Thermofisher). For replicative stress experiments, MMS was added to cultures at a final concentration of 0.03% and incubated for 5 hours before being processed for imaging.

### *sptPALM*

Live *S. pombe* cells were imaged with a custom-built microscope similar to that previously described<sup>51</sup>. The microscope is built around an inverted Olympus IX73 body fitted with a motorized stage (Prior H117E1I4) and a heated incubation chamber (Digital Pixel Ltd). Cells were illuminated using a 561-nm imaging laser (Cobolt, Jive) and a 405-nm activation laser (LaserBoxx, Oxxius). Both laser beams were expanded and collimated and were focused to the back focal plane (BFP) of an apochromatic 1.45 NA, 60× TIRF objective (Olympus, UIS2 APON 60× OTIRF). Both beams were angled in a highly inclined near-TIRF manner to achieve high signal-to-background. Illumination of the sample was controlled via mechanical shutters and all components were computer-controlled using the Micro-Manager software. The emission fluorescence from the sample was filtered with a band-pass filter (Semrock 593/40)

before being expanded to create an optimized image pixel size of 101 nm after projection onto the EMCCD camera (Photometrics Evolve 512 Delta).

Samples were mounted on microscope stage and incubated at 30°C. Cells were illuminated with continuous 561nm excitation (8.3mW at rear aperture of objective lens) and pulsed with 100ms 405nm laser illumination every 10s in order to photoconvert mEos3.2 molecules (max. 0.23mW at rear aperture of objective lens). Each experimental repeat consisted of data collection from 3 separate fields of view, imaged one after the other. Each acquisition consisted of 20,000 frames with a camera exposure time of 20ms.

### *sptPALM data analysis*

Raw sptPALM data was analysed using the ‘PeakFit’ plugin of the GDSC single-molecule localisation microscopy software package for Fiji (GDSC SMLM - <https://github.com/aherbert/gdsc-smlm>). Single molecules were identified and localised using a 2D gaussian fitting routine (configuration file available on request). Nuclear localisations consisting of a minimum of 20 photons and localised to a precision of 40nm or better were retained for further analysis. Single molecules were then tracked through time using the ‘Trace Diffusion’ GDSC SMLM plugin. Localisations appearing in consecutive frames within a threshold distance of 800nm were joined together into a trajectory<sup>51</sup>. Single molecule trajectories were then exported into .csv Spot-On format using the ‘Trace Exporter’ plugin.

Track data was uploaded into the Spot-On web interface and was analysed using the following jump length distribution parameters: Bin width ( $\mu\text{m}$ ) = 0.01, number of timepoints = 5, Jumps to consider = 4, Max jump ( $\mu\text{m}$ ) = 3. For Cnd2 (condensin) and all Smc5/6 components, data sets were fit with a 3-state Spot-On model using the default parameters, except for:  $D_{\text{slow}}$  min = 0.1, localisation error fit from data = yes,  $dZ$  ( $\mu\text{m}$ ) = 0.9. For cohesin data sets we fit a two-state model with the same parameters, excluding  $D_{\text{slow}}$ . In all cases, the model was fit to the cumulative distribution function (CDF). The decision by which model to fit was based on the Akaike information criterion reported by Spot-On (see figure S4).

Probability density function (PDF) histograms and model fit were created using data combined from all three repeats of an experiment and exported from Spot-On before being graphed in

Prism (GraphPad). Bar charts were produced by fitting data collected in each repeat (three fields of view) and extracting the fraction of bound molecules. Black circles represent the value derived for each repeat, bars represent the mean and error bars denote standard error of the mean. Two-tailed t-test was performed in Prism software of the Spot-On  $F_{\text{bound}}$  values from 3 repeats. Single-molecule localisation images were produced by plotting localisations with a precision of 30nm and were rendered with ImageJ 'Greys' lookup table and a final image pixel size of 20nm.

### *Structural modelling*

Sequence-threaded homology models for the head domains of both *S. pombe* Smc5 and Smc6 were generated using the PHYRE2 web portal<sup>52</sup>. The potential effects of introducing single point mutations were assessed using PyMOL (v2.32, The PyMOL Molecular Graphics System, Version 2.32, Schrödinger, LLC)

### *Yeast spot test assay*

Yeast strains were cultured in yeast extract (YE) overnight to mid-log phase. Cells were harvested and resuspended to a concentration of  $10^7$  cells/ml. Serial dilutions were then spotted onto YE agar plates containing the indicated genotoxic agent.

### *Yeast gross chromosomal rearrangement assay*

The rate of *ura4*<sup>+</sup> loss in the *RuraR* system was measured using a previously described fluctuation test<sup>45</sup>. Colonies growing on YNBA plates lacking uracil (and containing thiamine) were re-streaked onto YNBA plates containing uracil, either in the presence or absence of thiamine. After 5 days, 5 colonies were picked from either condition and each was grown to saturation (~48hrs) in 10ml liquid EMM culture containing uracil, with or without thiamine.

Each culture was counted and about  $1 \times 10^7$  cells were plated in triplicate on YEA plates containing 5'-fluoroorotic acid (5'-FOA; Melford). 100 $\mu$ l of a 1:20000 dilution of each saturated culture (about 200 cells) was plated in duplicate on YEA as titer plates. After 5 to 7 days of growth, 5-FOA resistant colonies and colonies on YEA were counted. A proportion of

5-FOA resistant colonies were streaked on YNBA lacking uracil to verify *ura4* gene function loss. These *ura4*- colonies were used in the translocation PCR assay. The rate of *ura4* loss per cell per generation was calculated using the Lea & Coulson method of the median<sup>53</sup>.

#### *mEos antibody production*

N-terminally 6XHis-tagged mEos2 was expressed from a pTWO-E vector in BL21(DE3) cells (Novagen). Cell pellets were suspended in 35ml buffer A (10mMTris, 100mMNaCl, 50mMNa<sub>2</sub>HPO<sub>4</sub>, pH8.0) with EDTA-free protease inhibitor mix (Roche) and AEBSF (10ug/ml) and lysed by sonication (Vibra-cell, Sonics) with 5 secs sonication and 10 seconds rest with a total sonication time of 3 minutes. Lysed cells were centrifuged at 18,500 rpm. (32,000g) and the supernatant was applied to a 5ml Ni-NTA agarose resin (Qiagen)(pre-equilibrated using buffer A) and incubated 1hr at 4°C. The column was washed with 8 column volumes of buffer B (50mM KH<sub>2</sub>PO<sub>4</sub>, 300mM NaCl, 20mM imidazole, 5% glycerol, pH7.9), and the protein was eluted with 2 column volumes of buffer C (50mMKH<sub>2</sub>PO<sub>4</sub>, 300mMNaCl, 250mM imidazole, 5% glycerol, pH7.9). The protein was further purified on an SD200 size exclusion column pre-equilibrated using buffer D (10mMTris, 100mMNaCl, 5% glycerol, pH8.0) and aliquots were snap frozen in liquid N<sub>2</sub> and stored at -80OC.

Purified mEos2 protein was used to raise custom rabbit antibodies (Eurogentec, Belgium). Immune sera from two rabbits were obtained and specific antibodies to mEos2 were affinity-purified on glutathione-sepharose columns bound with mEos2-GST. Antibody elution was carried out at acidic pH (0.1M glycine-Cl, pH 2.5) and then pH-neutralized to pH 7.0 with Tris-Cl, pH 8.8.

#### *Total cell extracts*

Logarithmically growing cells were harvested, washed in PBS, 20% trichloroacetic acid (TCA), then resuspended in 200µl of 20% TCA. Cells were ribolysed with glass beads and the cell homogenate was centrifuged at 14,000 for 10 min. The pellet was resuspended in 200µl of loading buffer (250 mM Tris-HCl [pH 8], 2% sodium dodecyl sulfate (SDS), 5% glycerol, 5% β-mercaptoethanol, 0.1% bromphenol blue) and boiled samples for 10min.

### *Immunoblotting*

Total cell extract samples were resolved by 8% SDS-PAGE, blotted onto Hybond ECL nitrocellulose membrane (Amersham Pharmacia biotech) and probed with custom rabbit polyclonal anti-mEos3 antibody (diluted 1:1000). Peroxidase-conjugated mouse-anti-rabbit secondary antibodies (diluted 1:5000, Dako A/S) were used to detect the primary antibody and these were revealed using an ECL detection kit (Amersham).

### *RuraR fluctuation assay*

The rate of *ura4*<sup>+</sup> loss in the *RuraR* system was measured using a fluctuation test as described previously<sup>45</sup>. Briefly, colonies growing on YNBA plates containing uracil, either in the presence or absence of thiamine were grown to saturation in 10ml liquid EMM culture containing uracil, with or without thiamine.

Each culture was counted and about  $1 \times 10^7$  cells were plated in triplicate on YEA plates containing 5'-fluoroorotic acid (5'-FOA; Melford). 100 $\mu$ l of a 1:20,000 dilution of each saturated culture (200 cells) was plated in duplicate on YEA as titer plates. After 6 days of growth colonies were counted. 5-FOA resistant colonies were streaked on YNBA lacking uracil (to verify *ura4* gene function loss) and on YEA before being used in the translocation PCR assay. The rate of *ura4* loss per cell per generation was calculated using the Lea & Coulson method of the median<sup>53</sup>.

## **Author contributions**

TJE, AWO, AMC and JMM conceived the experimental approach. TJE and MAO built the custom microscope. TJE acquired and analysed the microscopy data. AH wrote and benchmarked the PeakFit custom single-molecule software. TJE, DVC, AI, HQD and ATW performed strain construction, phenotypic analyses and molecular biology. AWO performed structural analysis and designed mutations. TJE, AWO, AMC and JMM wrote the manuscript.

## **Acknowledgements**

We would like to acknowledge Anders Hansen and Maxime Woringer for their help with initial implementation of the Spot-On software for analysis of sptPALM data in fission yeast. We thank Sarah Lambert for control strains for the GCR assay and Steven F. Lee for single-molecule microscopy advice and proof-reading of the manuscript. We also thank J. Palecek for the *nse3-R254E* strain. AMC acknowledges support from the Wellcome trust (110047/Z/15/Z), JMM and AWO acknowledge support from the MRC (MR/P018955/1). TJE would like to dedicate this manuscript to the memory of Vivien Horobin.

## Figure legends

### Figure 1

*Implementation of sptPALM to monitor SMC chromatin association in live cells.*

A. Schematic representation of the three SMC complexes in fission yeast and their core components.

B. Immunoblot of *S. pombe* whole cell extracts to confirm expression of the different kleisin-mEos3 fusion proteins. Black arrow head indicates position of Rad21-mEos3.

C. Brightfield and cumulative single-molecule localisation images (20,000 frames) of Cnd2-mEos3 expressing cells in an asynchronous culture. Scale bar = 2 $\mu$ m.

D. Probability density function (PDF) histograms of Cnd2-mEos3 single-molecule displacements for multiple  $\Delta t$ . Data are from 3 pooled independent experiments, each with three technical repeats. Dashed line indicates fit derived from CDF model fitting in Spot-On.

E. Fraction of bound molecules derived from Spot-On model fitting. Mean (+/- S.E.M). Black dots indicate Spot-On  $F_{\text{bound}}$  values derived from 3 independent experiments. \*\*\* =  $p < 0.001$ .

## Figure 2

*sptPALM analysis of the Smc5/6 and cohesin kleisin subunits, Nse4 and Rad21.*

A. Probability density function (PDF) histograms and Spot-On model fitting for Nse4-mEos3 (Smc5/6) and Rad21-mEos3 (cohesin) single-molecule displacements. Data are from 3 pooled independent experiments, each with three technical repeats.

B.  $F_{\text{bound}}$  values derived from Spot-On model fitting data in A. Mean (+/- S.E.M). Black dots: values derived from 3 independent experiments. \*\*\*\* =  $p < 0.0001$

C. Representative images of nuclear Nse4-mEos3 or Rad21-mEos3 single-molecule localisations detected in A. Dashed line indicates cropped nuclear region. Scale bar =  $1\mu\text{m}$

### Figure 3

*Differential requirements of Nse6 and Brc1 for Smc5/6 chromatin association.*

A. Schematic diagram of Smc5/6 recruitment to  $\gamma$ -H2A (red dots: H2A phosphorylation) at stalled replication forks via Brc1 and Nse6 interaction. Yellow star indicates a DNA lesion.

B. Comparison of Nse4-mEos3 and Nse6-mEos3  $F_{\text{bound}}$  values derived from Spot-On fitting of sptPALM displacement histograms (see figure S1C for displacement histograms). Mean +/- S.E.M. Black dots values derived from 3 independent experiments. \*\* =  $p < 0.01$

C. Displacement PDF histograms from asynchronous cells expressing Nse4-mEos3 in *brc1Δ* and *nse6Δ* genetic backgrounds. Data are from 3 pooled independent experiments, each with three technical repeats. Spot-On model fit is denoted by dashed line.

D. Fraction of bound molecules extracted from Spot-On model fits from C. Mean +/- S.E.M. Black dots denote independent repeats. \*\* =  $p < 0.01$ , \*\*\*\* =  $p < 0.0001$

E.  $F_{\text{Bound}}$  fraction values from D compared to parallel experiments where cells were treated with 0.03% MMS for 5 hours. Mean +/- S.E.M. Black dots denote independent repeats. \* =  $p < 0.05$ , *ns* = not significant.

F. Comparison of  $F_{\text{Bound}}$  fraction values from Nse4-mEos3 sptPALM in *brc1Δ* and *hta1-SA hta2-SA* mutant genetic backgrounds. Black dots denote independent experiments. \*\* =  $p < 0.01$

## Figure 4

*Smc5/6 ATPase activity regulates chromatin association.*

A. Schematic representation of SMC head engagement upon ATP binding.

B. Comparison of the fraction of bound molecules from Nse4-mEos3 sptPALM experiments in asynchronous *smc6-R150A* and *smc5-R77A* genetic backgrounds to wild type dataset. Mean +/- S.E.M. Black dots denote independent repeats. \*\* =  $p < 0.01$ , \*\*\* =  $p < 0.001$

C. Secondary structure molecular cartoons of homology models for the head domains of *S. pombe* Smc6, highlighting the arginine finger and its interaction with ATP. The X-ray crystal structure for the head domain of *Pyrococcus furiosus* SMC in complex with ATP served as a reference, providing the expected position of bound ATP the homology model. Key amino acids are shown in 'stick representation'. The lower panel shows the predicted increase in severity of steric clashes made with the arginine finger through introduction of each of the indicated mutations.

D. Yeast spot assay of *S. pombe* strains harbouring different *smc6* ATPase mutations grown at 30°C for 3 days.

E. Fraction of chromatin bound molecules in each of the *smc6-T135* mutant backgrounds compared to a wild type data set and *smc6-74* (A151T). Mean +/- S.E.M. Black dots denote independent repeats. \* =  $p < 0.05$ , \*\* =  $p < 0.01$ , \*\*\* =  $p < 0.001$

## Figure 5

*Double strand, but not single strand, DNA binding is required for Smc5/6 chromatin association.*

A. Schematic representation of the regions of known DNA interaction in *S. pombe* Smc5/6.

B. Probability density function histogram (three independent experiments, each with three technical repeats) and Spot-On model fit for Nse4-mEos3 in *nse3-R254E* background and the resulting fraction of bound molecules compared to wild type data set. Bar chart shows mean +/- S.E.M. Black dots denote independent repeats. \*\*\* =  $p < 0.001$

C. Schematic diagram of the *S. pombe* hinge region adapted from<sup>19</sup>. Residues implicated in ssDNA interaction are highlighted with red filled circles.

D. Fraction of bound Nse4-mEos3 derived from sptPALM experiments in Smc5/6 hinge mutant backgrounds compared to wild type dataset. Mean +/- S.E.M. Black dots denote independent repeats.

E. Fraction of bound Nse4-mEos3 extracted from sptPALM of Nse4-mEos3 in *smc6* hinge mutants treated with 0.03% MMS for 5 hours. Compared to asynchronous untreated datasets from D. Mean +/- S.E.M. Black dots denote independent repeats. \* =  $p < 0.05$ ,

## Figure 6

*ssDNA binding activity is required to prevent gross chromosomal re-arrangements.*

A. Diagram of the site specific replication stall system *RTS1-ura4-RTS1*<sup>45</sup>, which consists of two inverted *RTS1* sequences integrated on either sides of the *ura4* gene. Rtf1 binds the *RTS1* sequence and stalls incoming replication forks coming from both centromeric and telomeric sides. Rtf1 is expressed under the control of the *nmt41* promoter which is “off” in the presence of thiamine and “on” upon thiamine removal.

B. Induction of *rtf1* in cells harbouring *RuraR* construct induces *ura4* marker loss as assayed by 5-FOA resistance. Marker loss may be due to point mutations resulting from replication slippage or full deletions of *ura4* and translocations between *RTS1* on chromosome III (*RuraR*) and the native *RTS1* at the *mat* locus on chromosome II, both resulting from non-allelic recombination. Left: *ura4* marker loss per cell per generation. Cells growing in the presence (+thi, arrest repressed) or absence (-thi, arrest induced) of thiamine were analysed by fluctuation analysis. *smc6-74* shows minimal increase in *ura4* loss when *nmt41-rtf1* is on, whereas *smc6-X* shows increased *ura4* loss when *nmt41-rtf1* is off and a major *ura4* loss increase when *nmt41-rtf1* is on. Middle: RFB-induced deletions per cell per generation and Right: RFB-induced translocations per cell per generation. Deletions and translocations were identified by PCR assay performed on 5-FOA resistant colonies (see Supplementary figure 3).

C. Schematic diagram of Smc5/6 DNA interactions and their roles (left) and proposed model of Smc5/6 chromatin association (right). Loading requires dsDNA binding by Nse3 and Smc5 and Smc6 ATPase activity. ssDNA binding at the hinge is not required for loading but is required for subsequent functions to regulate homologous recombination, suppress non-allelic recombination and GCRs. Smc5/6 association with chromatin is dependent on Nse5 and Nse6 and either Brc1-independent (bottom) or Brc1-dependent via recruitment to  $\gamma$ -H2A (top). Nse5/6 may act either to directly load Smc5/6 (i.e. top), or may stabilise its association after initial loading by dsDNA interaction (i.e. bottom)

## Supplementary Figure 1

*Characterisation of mEos3 tagged Smc5/6, condensin and cohesin subunits.*

A. Spot assay of *S. pombe* strains expressing different SMC components fused to the mEos3 fluorescent tag. Plates were incubated at 30°C for 3 days.

B. Whole cell single molecule localisation images of Nse4-mEos3 and Rad21-mEos3 expressing fission yeast demonstrating clear nuclear localisation of the proteins. Dashed white line indicates cell wall. Scale bar = 1  $\mu\text{m}$ .

C. PDF histograms of single-molecule displacements for multiple  $\Delta t$  of alternative cohesin (Smc1) and Smc5/6 (Smc6, Nse2 and Nse6) subunits. Data are pooled from 3 individual experiments each with three technical repeats. Dashed line indicates model derived from CDF fitting in Spot-On.

D. Fractions of bound molecules calculated from Spot-On model fitting data in C. Mean ( $\pm$  S.E.M). Black dots indicate Spot-On  $F_{\text{bound}}$  values derived from 3 independent experimental datasets.

## Supplementary Figure 2

*Smc5/6 behaviour fits a 3-state model.*

A. PDF histograms of single-molecule displacements for Nse4-mEos3 and Rad21-mEos3 over multiple  $\Delta t$  fit with either a 2-state or 3-state Spot-On model. Data are pooled from 3 independent experiments, each with three technical repeats. Dashed line indicates model derived from CDF fitting in Spot-On.

B. Akaike information criterion (AIC) scores from Spot-On model fitting in A. Nse4-mEos3 3-state fitting showed a large difference in AIC scores compared to 2-state fitting. This indicates the data are best described by a 3-state model. The difference in AIC scores for Rad21-mEos3 was much smaller and thus a 2-state model was used.

C. Fractions of the total population of molecules observed residing in each kinetic state extracted from Spot-On model fitting data in A.

D. Apparent diffusion coefficients of Spot-On sub-populations of Nse4-mEos3 (3-State) and Rad21-mEos3 (2-State).

### Supplementary Figure 3

*Characterisation of mEos3 tagged Smc5/6 ATPase mutants.*

A. Spot assay of *S. pombe* strains harbouring arginine finger mutations in either *smc5* or *smc6*.

Plates were incubated at 30°C for 3 days.

B. PDF histograms of single-molecule displacements for multiple  $\Delta t$  of Nse4-mEos3 for *smc5* (R77A) or *smc6* (R150A) arginine finger mutants (see figure 4B for fraction bound).

Dashed line indicates model derived from CDF fitting in Spot-On. Data are pooled from 3 individual experiments, each with 3 technical repeats.

C. PDF histograms of single-molecule displacements for multiple  $\Delta t$  of Nse4-mEos3 in the indicated mutants (see figure 4E for fraction bound). Dashed line indicates model derived from CDF fitting in Spot-On. Data are pooled from 3 individual experiments, each with 3 technical repeats.

D. Fraction of bound molecules extracted from sptPALM of Nse4-mEos3 in *smc6* ATPase mutants treated with 0.03% MMS for 5 hours compared to asynchronous untreated datasets.

Mean +/- S.E.M. Black dots denote independent repeats. \* =  $p < 0.05$ , *ns* = not significant

## Supplementary Figure 4

*Analysis of the consequences of site-specific replication fork stalling on cell viability and gross chromosomal re-arrangements.*

**A.** Yeast spot assay of *S. pombe* strains harbouring the site-specific replication stall system *RuraR*. Replication fork stalling at *RTS1* is induced in the absence of thiamine (on). Plates were incubated at 30°C for 3 days.

**B.** PCR-based assay for translocation between *RTS1* at *RuraR* and the native *RTS1* at the mating type locus in *ura4<sup>-</sup>* colonies generated in the *ura4* loss of gene function assay. Schematic to show the three primer pairs used. One pair (red arrows) amplifies the junction resulting from ectopic recombination between chromosome II and III (TLII/III). The second pair (grey arrows) amplifies the *ura4* locus to distinguish point mutations, truncations (internal deletions) and full-length deletions. *rng3* (blue arrows), an essential gene located between *RuraR* and the telomere, is amplified as positive control.

**C.** Example of control PCRs (top) and PCRs of 5-FOA resistant/*ura4<sup>-</sup>* colonies (bottom). The *rng3* product is amplified in all strains, but not in the negative control (“-”). *ura4* is amplified only in a *RuraR* strain, but not in Wild type (wt) (harbours full deletion of *ura4*, *ura4-D18*), the translocation positive control (“+”, gift from S. Lambert<sup>45</sup>) or the negative control. Translocation between chromosome II and III can only be detected in the positive control.

## Supplementary Figure 5

*Repeat of fluctuation assay as in Figure 6. ura4 marker loss per cell per generation.*

## References

1. Uhlmann, F. SMC complexes: from DNA to chromosomes. *Nat. Rev. Mol. Cell Biol.* **17**, 399–412 (2016).
2. Murray, J. M. & Carr, A. M. Smc5/6: A link between DNA repair and unidirectional replication? *Nat. Rev. Mol. Cell Biol.* **9**, 177–182 (2008).
3. Aragón, L. The Smc5/6 Complex: New and Old Functions of the Enigmatic Long-Distance Relative. *Annu. Rev. Genet.* **52**, 89–107 (2018).
4. Irmisch, A., Ampatzidou, E., Mizuno, K., O’Connell, M. J. & Murray, J. M. Smc5/6 maintains stalled replication forks in a recombination-competent conformation. *EMBO J.* **28**, 144–155 (2009).
5. Menolfi, D., Delamarre, A., Lengronne, A., Pasero, P. & Branzei, D. Essential Roles of the Smc5/6 Complex in Replication through Natural Pausing Sites and Endogenous DNA Damage Tolerance. *Mol. Cell* **60**, 835–846 (2015).
6. Xue, X. *et al.* Restriction of Replication Fork Regression Activities by a Conserved SMC Complex. *Mol. Cell* **56**, 436–445 (2014).
7. Bonner, J. N. *et al.* Smc5/6 Mediated Sumoylation of the Sgs1-Top3-Rmi1 Complex Promotes Removal of Recombination Intermediates. *Cell Rep.* **16**, 368–378 (2016).
8. Jeppsson, K. *et al.* The Chromosomal Association of the Smc5/6 Complex Depends on Cohesion and Predicts the Level of Sister Chromatid Entanglement. *PLoS Genet.* **10**, e1004680 (2014).
9. Bentley, P., Tan, M. J. A., McBride, A. A., White, E. A. & Howley, P. M. The SMC5/6 Complex Interacts with the Papillomavirus E2 Protein and Influences Maintenance of Viral Episomal DNA. *J. Virol.* (2018) doi:10.1128/jvi.00356-18.
10. Niu, C. *et al.* The Smc5/6 complex restricts HBV when localized to ND10 without inducing an innate immune response and is counteracted by the HBV X protein shortly after infection. *PLoS ONE* vol. 12 (2017).
11. De Piccoli, G. *et al.* Smc5-Smc6 mediate DNA double-strand-break repair by promoting sister-chromatid recombination. *Nat. Cell Biol.* **8**, 1032–1034 (2006).
12. Bermúdez-López, M. *et al.* The Smc5/6 complex is required for dissolution of DNA-mediated sister chromatid linkages. *Nucleic Acids Res.* **38**, 6502–6512 (2010).
13. Hirano, M. & Hirano, T. Opening closed arms: Long-distance activation of SMC ATPase by hinge-DNA interactions. *Mol. Cell* **21**, 175–186 (2006).
14. Diebold-Durand, M. L. *et al.* Structure of Full-Length SMC and Rearrangements Required for Chromosome Organization. *Mol. Cell* **67**, 334–347.e5 (2017).
15. Muir, K. W., Li, Y., Weis, F. & Panne, D. The structure of the cohesin ATPase elucidates the mechanism of SMC–kleisin ring opening. *Nat. Struct. Mol. Biol.* **27**, 233–239 (2020).

16. Elbatsh, A. M. O. *et al.* Cohesin Releases DNA through Asymmetric ATPase-Driven Ring Opening. *Mol. Cell* **61**, 575–588 (2016).
17. Terakawa, T. *et al.* The condensin complex is a mechanochemical motor that translocates along DNA. *Science (80-. )*. **358**, 672–676 (2017).
18. Elbatsh, A. M. O. *et al.* Distinct Roles for Condensin’s Two ATPase Sites in Chromosome Condensation. *Mol. Cell* **76**, 724–737.e5 (2019).
19. Alt, A. *et al.* Specialized interfaces of Smc5/6 control hinge stability and DNA association. *Nat. Commun.* **8**, (2017).
20. Doyle, J. M., Gao, J., Wang, J., Yang, M. & Potts, P. R. MAGE-RING protein complexes comprise a family of E3 ubiquitin ligases. *Mol. Cell* **39**, 963–974 (2010).
21. Zabradý, K. *et al.* Chromatin association of the SMC5/6 complex is dependent on binding of its NSE3 subunit to DNA. *Nucleic Acids Res.* **44**, 1064–1079 (2016).
22. Varejão, N. *et al.* DNA activates the Nse2/Mms21 SUMO E3 ligase in the Smc5/6 complex. *EMBO J.* **37**, 1–16 (2018).
23. Pebernard, S., Wohlschlegel, J., McDonald, W. H., Yates, J. R. & Boddy, M. N. The Nse5-Nse6 Dimer Mediates DNA Repair Roles of the Smc5-Smc6 Complex. *Mol. Cell. Biol.* **26**, 1617–1630 (2006).
24. Taylor, E. M., Copsey, A. C., Hudson, J. J. R., Vidot, S. & Lehmann, A. R. Identification of the Proteins, Including MAGEG1, That Make Up the Human SMC5-6 Protein Complex. *Mol. Cell. Biol.* **28**, 1197–1206 (2008).
25. Ocampo-Hafalla, M. T. & Uhlmann, F. Cohesin loading and sliding. *J. Cell Sci.* **124**, 685–691 (2011).
26. Oravcová, M. *et al.* Brc1 Promotes the Focal Accumulation and SUMO Ligase Activity of Smc5-Smc6 during Replication Stress. *Mol. Cell. Biol.* **39**, 1–15 (2018).
27. Wan, B., Wu, J., Meng, X., Lei, M. & Zhao, X. Molecular Basis for Control of Diverse Genome Stability Factors by the Multi-BRCT Scaffold Rtt107. *Mol. Cell* (2019) doi:10.1016/j.molcel.2019.05.035.
28. Räschle, M. *et al.* Proteomics reveals dynamic assembly of Repair complexes during bypass of DNA cross-links. *Science (80-. )*. **348**, (2015).
29. Pebernard, S., Schaffer, L., Campbell, D., Head, S. R. & Boddy, M. N. Localization of Smc5/6 to centromeres and telomeres requires heterochromatin and SUMO, respectively. *EMBO J.* **27**, 3011–3023 (2008).
30. Lindroos, H. B. *et al.* Chromosomal Association of the Smc5/6 Complex Reveals that It Functions in Differently Regulated Pathways. *Mol. Cell* **22**, 755–767 (2006).
31. Manley, S. *et al.* High-density mapping of single-molecule trajectories with photoactivated localization microscopy. *Nat. Methods* **5**, 155–157 (2008).
32. Uphoff, S., Reyes-Lamothe, R., De Leon, F. G., Sherratt, D. J. & Kapanidis, A. N. Single-

- molecule DNA repair in live bacteria. *Proc. Natl. Acad. Sci. U. S. A.* **110**, 8063–8068 (2013).
33. Sutani, T. *et al.* Fission yeast condensin complex: Essential roles of non-SMC subunits for condensation and Cdc2 phosphorylation of Cut3/SMC4. *Genes Dev.* **13**, 2271–2283 (1999).
  34. Hansen, A. S. *et al.* Robust model-based analysis of single-particle tracking experiments with spot-on. *Elife* **7**, 1–33 (2018).
  35. Woringer, M., Izeddin, I., Favard, C. & Berry, H. Anomalous Subdiffusion in Living Cells: Bridging the Gap Between Experiments and Realistic Models Through Collaborative Challenges. *Front. Phys.* **8**, 1–9 (2020).
  36. Williams, J. S. *et al.*  $\gamma$ H2A binds Brcl to maintain genome integrity during S-phase. *EMBO J.* (2010) doi:10.1038/emboj.2009.413.
  37. Nakamura, T. M., Du, L.-L., Redon, C. & Russell, P. Histone H2A Phosphorylation Controls Crb2 Recruitment at DNA Breaks, Maintains Checkpoint Arrest, and Influences DNA Repair in Fission Yeast. *Mol. Cell. Biol.* (2004) doi:10.1128/mcb.24.14.6215-6230.2004.
  38. Verkade, H. M., Bugg, S. J., Lindsay, H. D., Carr, A. M. & O’Connell, M. J. Rad18 is required for DNA repair and checkpoint responses in fission yeast. *Mol. Biol. Cell* **10**, 2905–2918 (1999).
  39. Fousteri, M. I. A novel SMC protein complex in *Schizosaccharomyces pombe* contains the Rad18 DNA repair protein. *EMBO J.* (2000) doi:10.1093/emboj/19.7.1691.
  40. Lammens, A., Schele, A. & Hopfner, K. P. Structural biochemistry of ATP-driven dimerization and DNA-stimulated activation of SMC ATPases. *Curr. Biol.* (2004) doi:10.1016/j.cub.2004.09.044.
  41. Ampatzidou, E., Irmisch, A., O’Connell, M. J. & Murray, J. M. Smc5/6 Is Required for Repair at Collapsed Replication Forks  $\nabla$ . *Mol. Cell. Biol.* **26**, 9387–9401 (2006).
  42. Outwin, E. A., Irmisch, A., Murray, J. M. & O’Connell, M. J. Smc5-Smc6-Dependent Removal of Cohesin from Mitotic Chromosomes. *Mol. Cell. Biol.* **29**, 4363–4375 (2009).
  43. Hassler, M. *et al.* Structural Basis of an Asymmetric Condensin ATPase Cycle. *Mol. Cell* **74**, 1175–1188.e9 (2019).
  44. Dalgaard, J. Z. & Klar, A. J. S. A DNA replication-arrest site RTS1 regulates imprinting by determining the direction of replication at *mat1* in *S. pombe*. *Genes Dev.* (2001) doi:10.1101/gad.200801.
  45. Lambert, S., Watson, A., Sheedy, D. M., Martin, B. & Carr, A. M. Gross chromosomal rearrangements and elevated recombination at an inducible site-specific replication fork barrier. *Cell* (2005) doi:10.1016/j.cell.2005.03.022.
  46. Mizuno, K., Miyabe, I., Schalbetter, S. A., Carr, A. M. & Murray, J. M. Recombination-restarted replication makes inverted chromosome fusions at inverted repeats. *Nature* **493**, 246–249 (2013).

47. Iraqui, I. *et al.* Recovery of Arrested Replication Forks by Homologous Recombination Is Error-Prone. *PLoS Genet.* (2012) doi:10.1371/journal.pgen.1002976.
48. Murayama, Y., Samora, C. P., Kurokawa, Y., Iwasaki, H. & Uhlmann, F. Establishment of DNA-DNA Interactions by the Cohesin Ring. *Cell* **172**, 465-477.e15 (2018).
49. Furuya, K., Takahashi, K. & Yanagida, M. Faithful anaphase is ensured by Mis4, a sister chromatid cohesion molecule required in S phase and not destroyed in G1 phase. *Genes Dev.* (1998) doi:10.1101/gad.12.21.3408.
50. Watson, A. T., Garcia, V., Bone, N., Carr, A. M. & Armstrong, J. Gene tagging and gene replacement using recombinase-mediated cassette exchange in *Schizosaccharomyces pombe*. *Gene* **407**, 63–74 (2008).
51. Etheridge, T. J. *et al.* Quantification of DNA-associated proteins inside eukaryotic cells using single-molecule localization microscopy. *Nucleic Acids Res.* **42**, (2014).
52. Kelley, L. A., Mezulis, S., Yates, C. M., Wass, M. N. & Sternberg, M. J. E. The Phyre2 web portal for protein modeling, prediction and analysis. *Nat. Protoc.* (2015) doi:10.1038/nprot.2015.053.
53. Lea, D. E. & Coulson, C. A. The distribution of the numbers of mutants in bacterial populations. *J. Genet.* (1949) doi:10.1007/BF02986080.

Figure 1

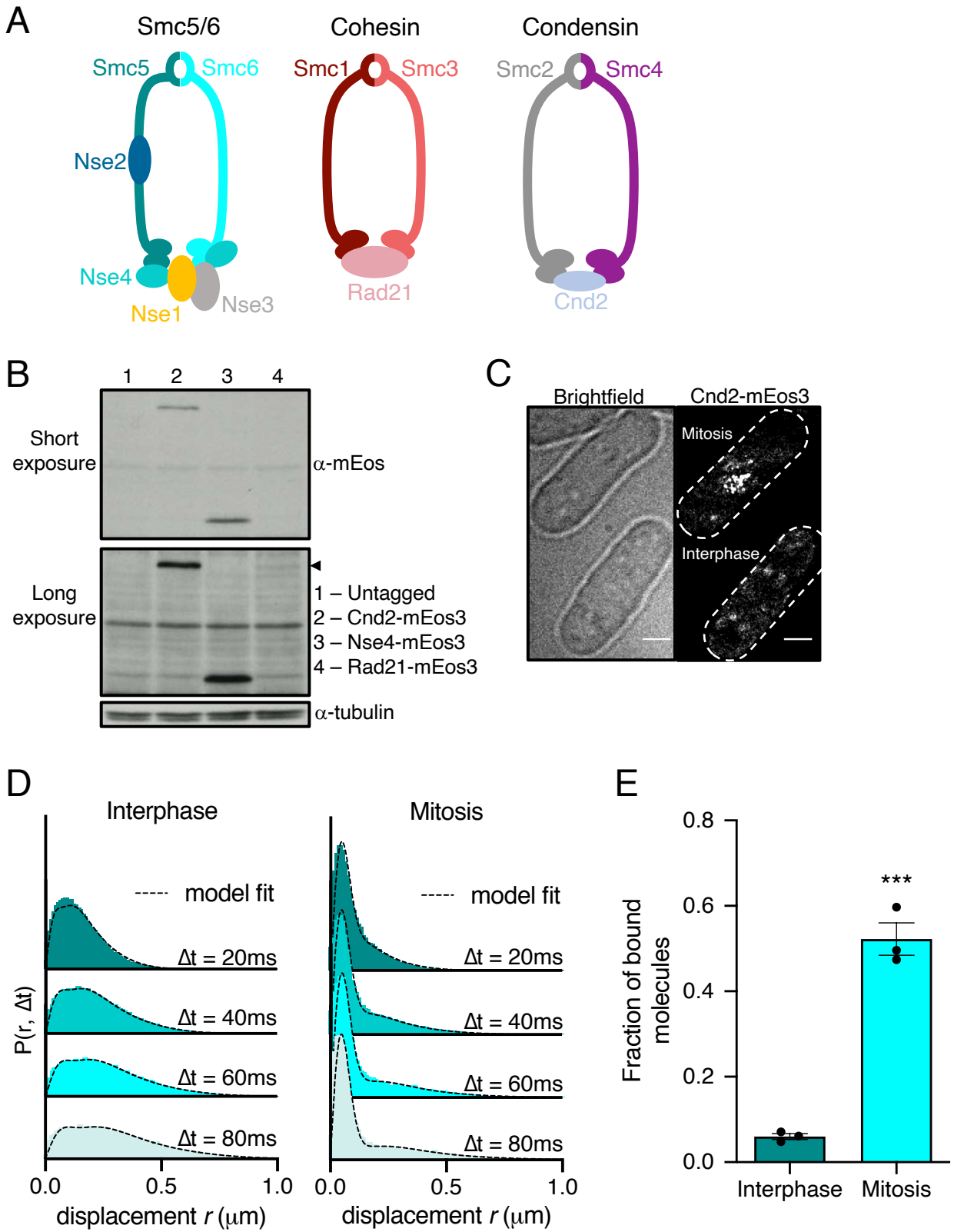


Figure 2

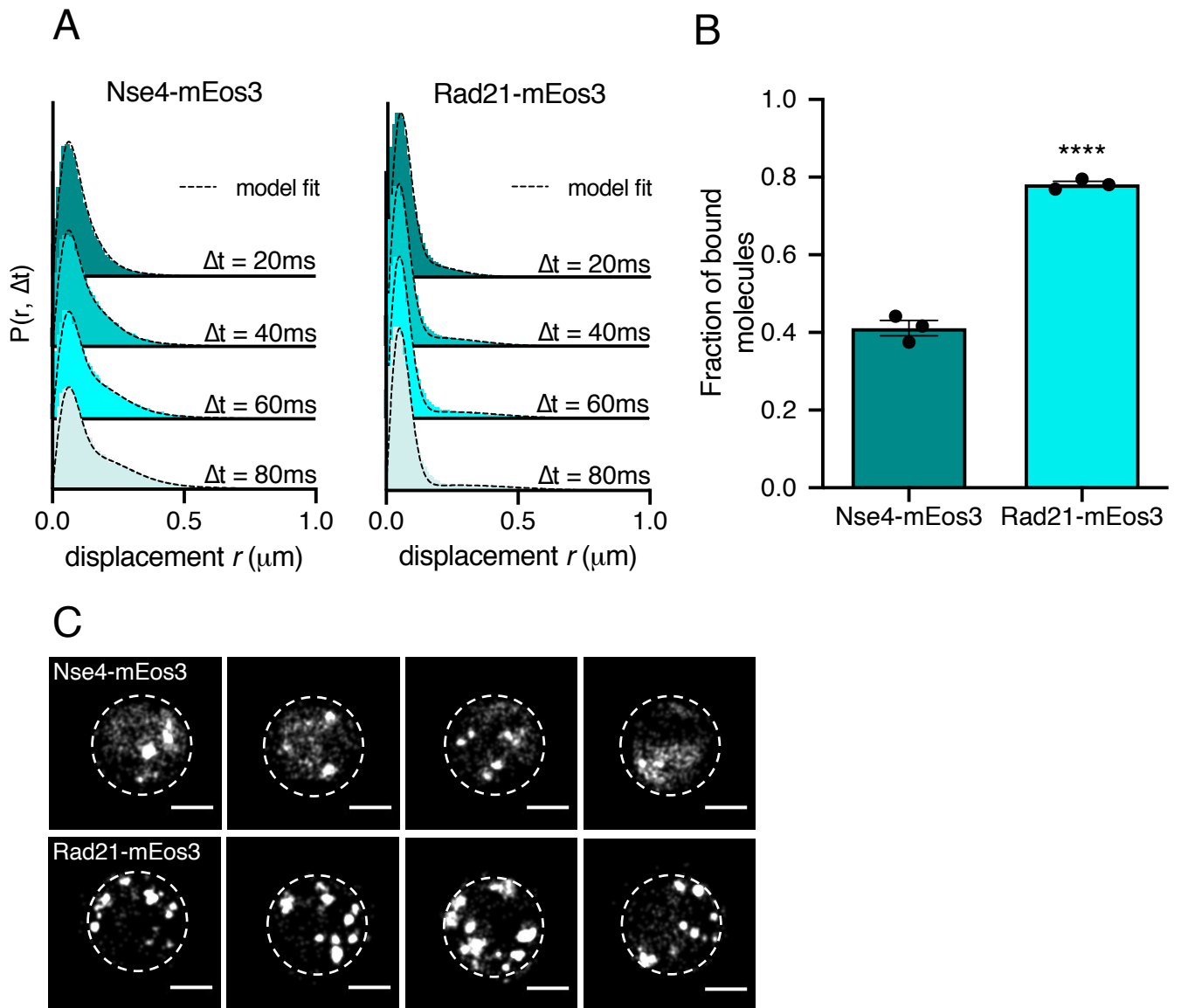


Figure 3

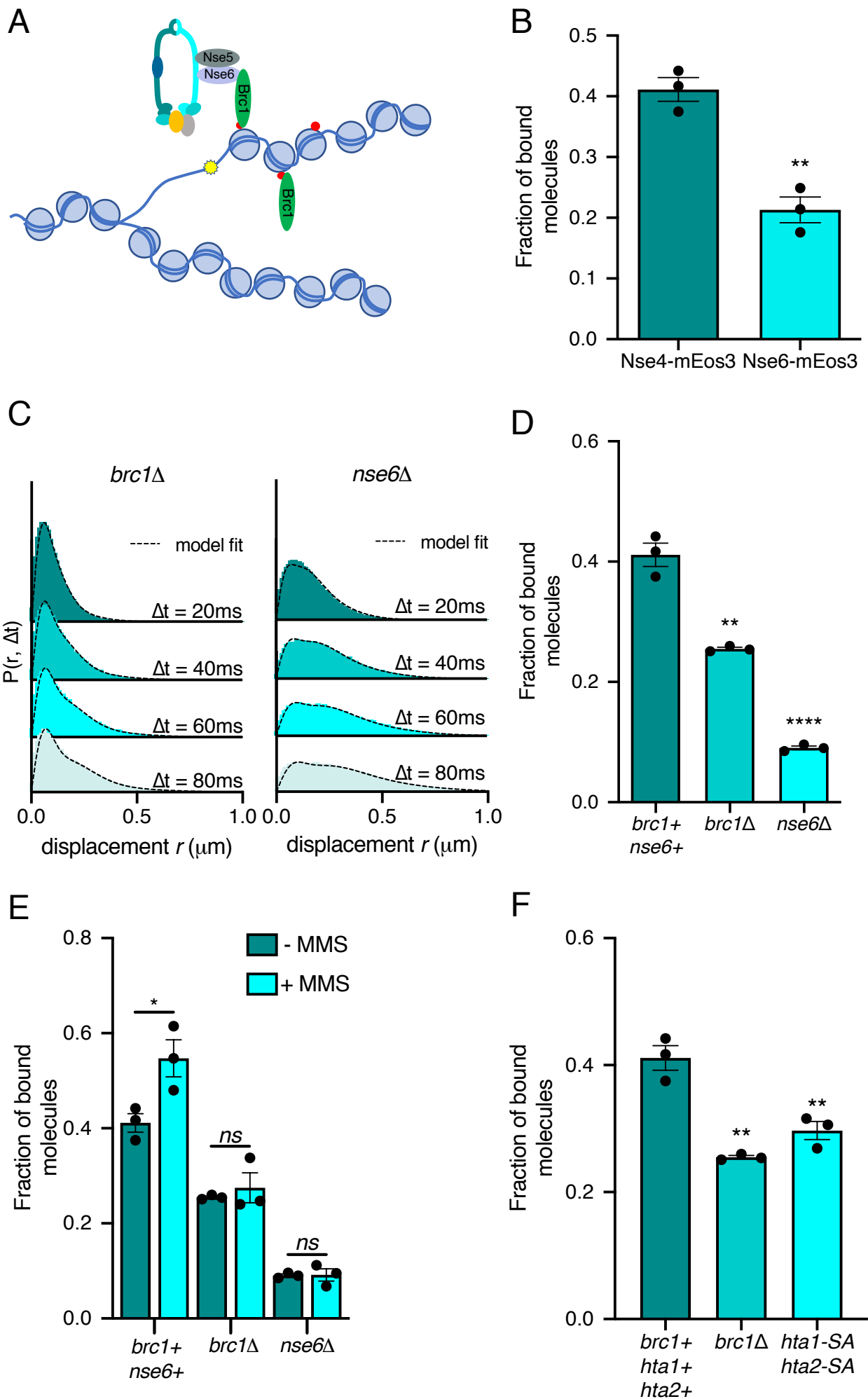
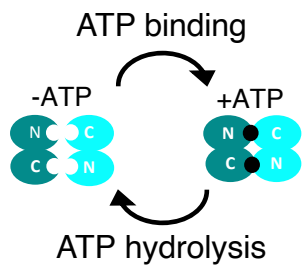
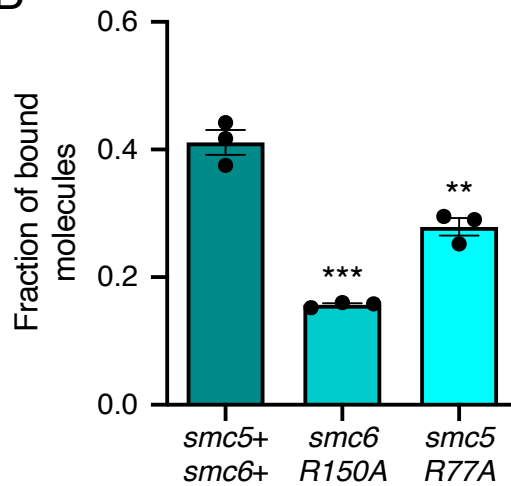


Figure 4

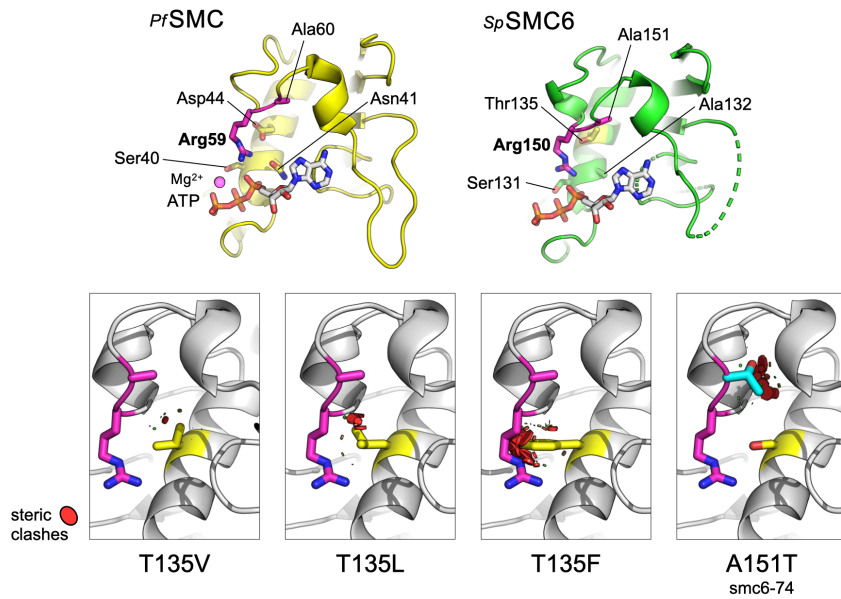
A



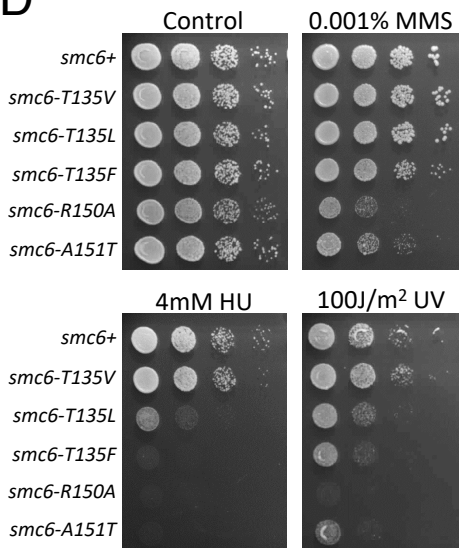
B



C



D



E

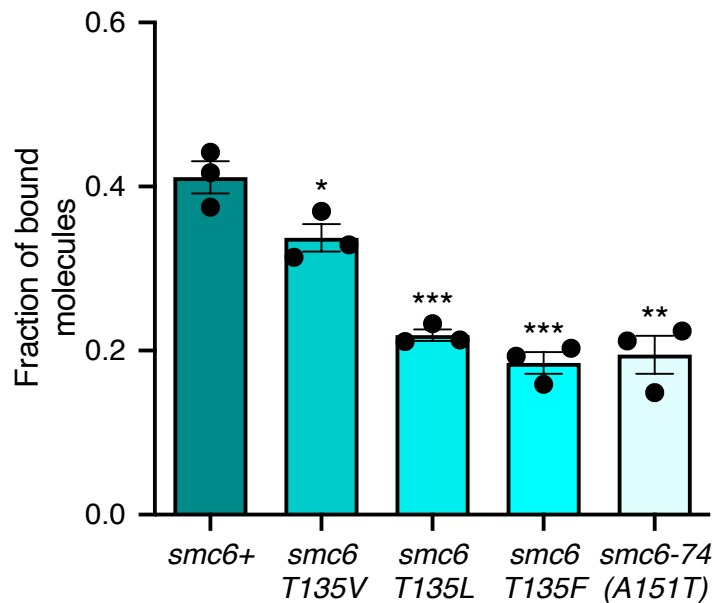


Figure 5

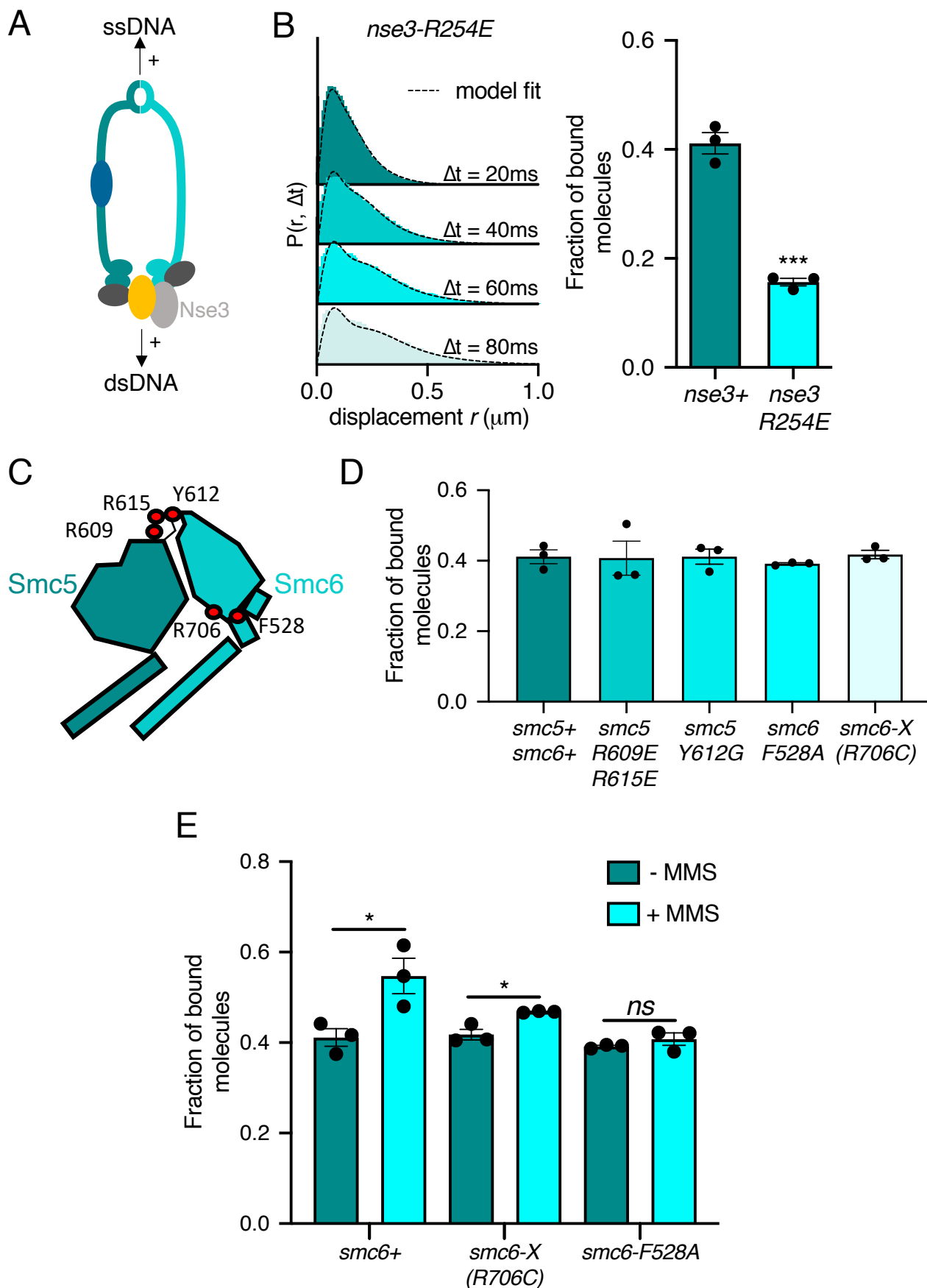
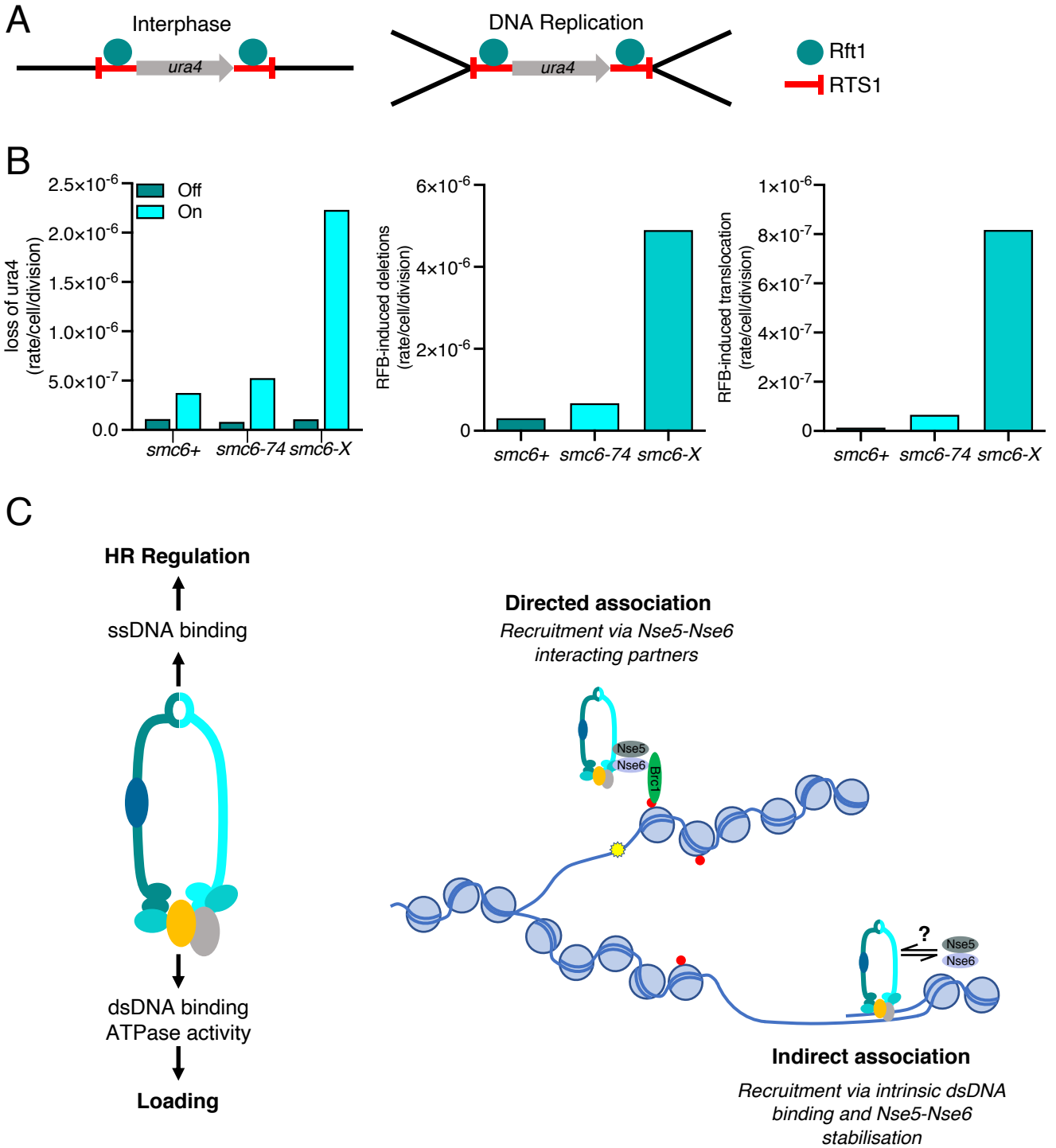
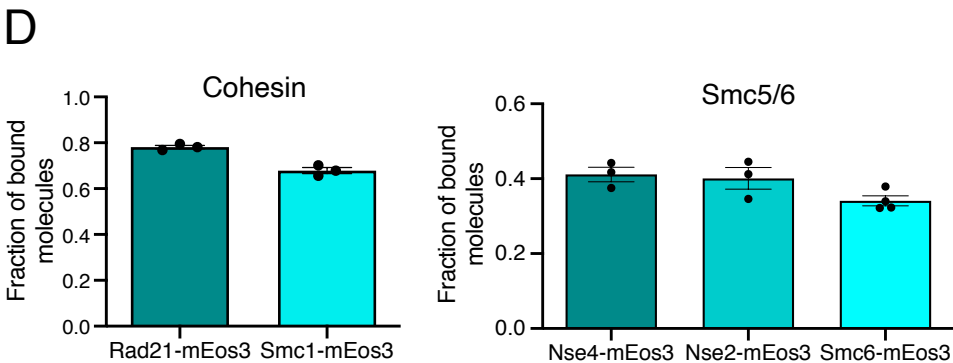
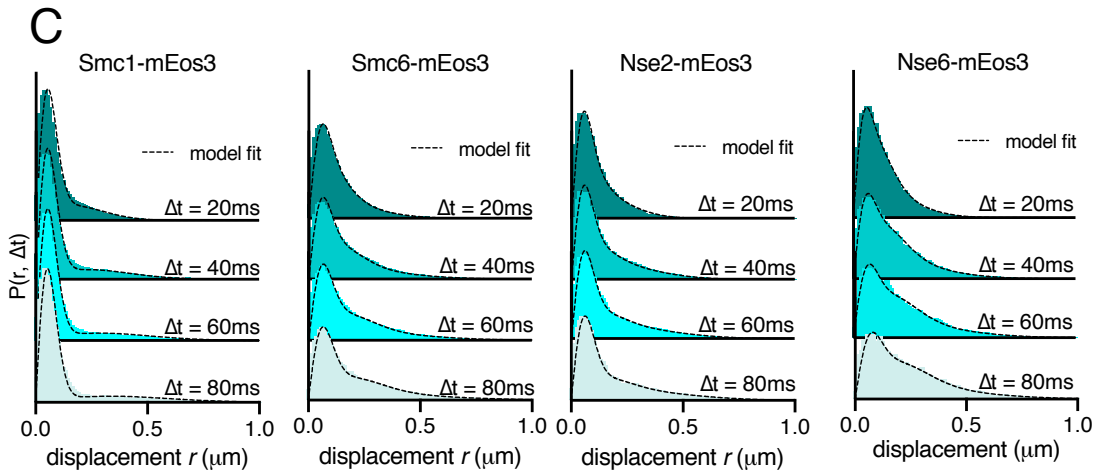
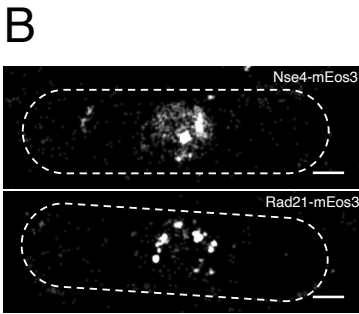
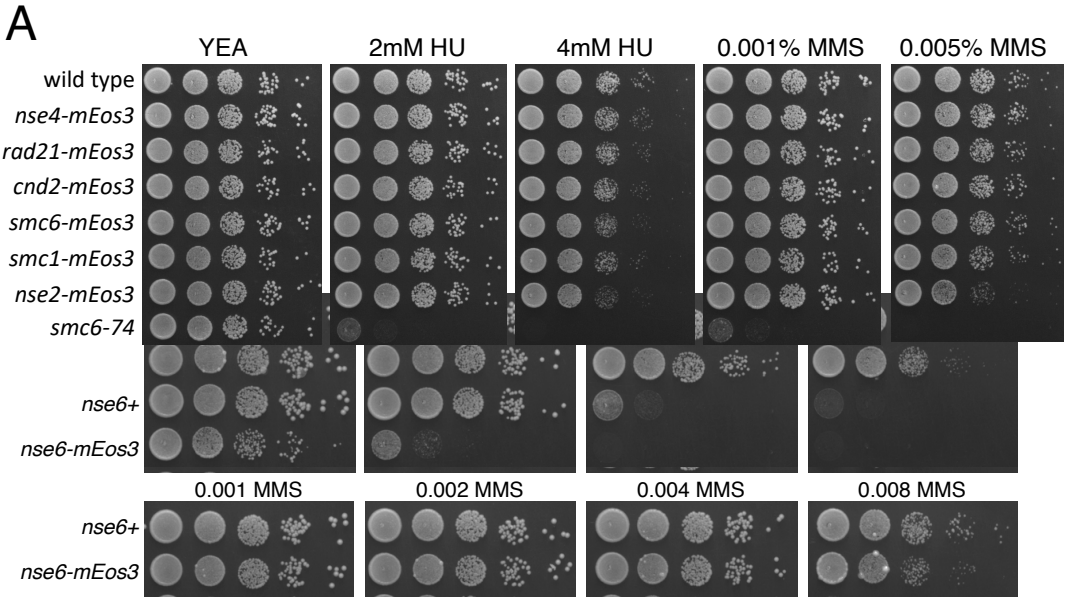


Figure 6

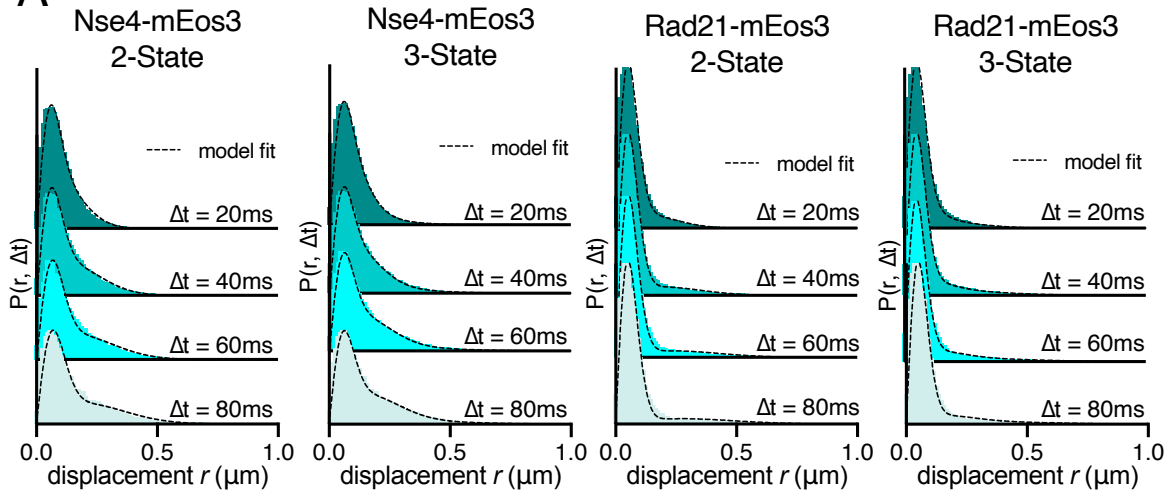


# Supplementary Figure 1



# Supplementary Figure 2

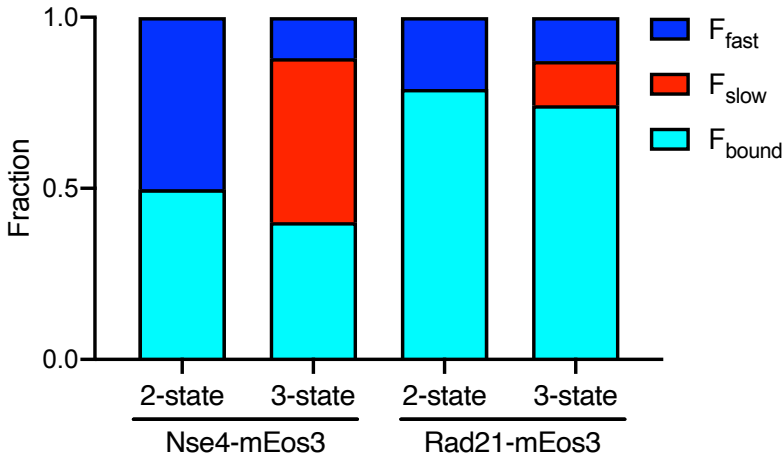
**A**



**B**

Akaike information criterion (AIC)		
Strain	2-State	3-State
Nse4-mEos3	-130,870.50	-144,755.61
Rad21-mEos3	-130,529.27	-135,461.01

**C**

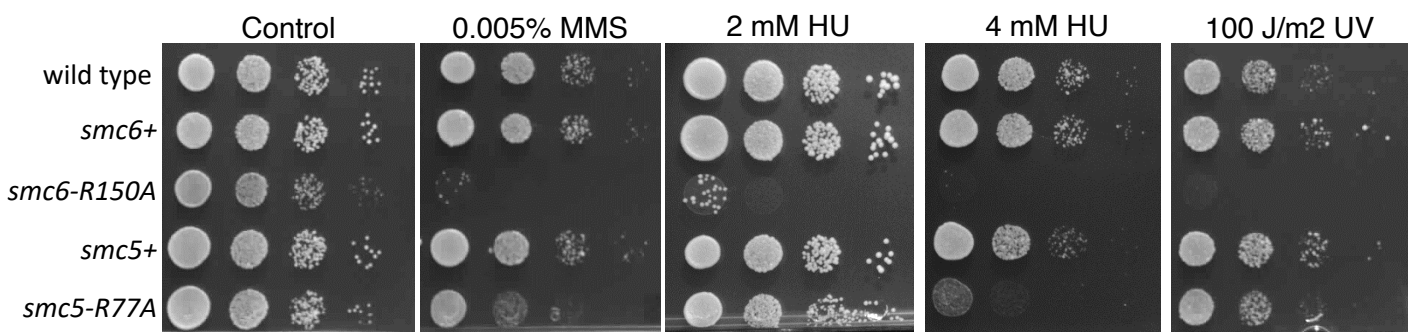


**D**

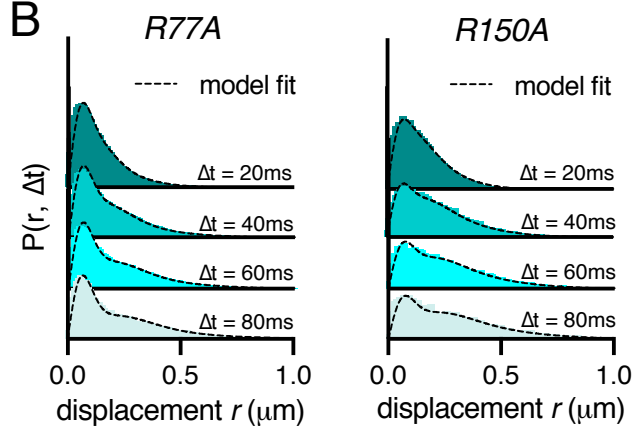
Apparent diffusion coefficient ( $\mu\text{m}^2/\text{s}$ )			
Strain	$D_{\text{bound}}$	$D_{\text{slow}}$	$D_{\text{fast}}$
Nse4-mEos3	$0.005 \pm 0.001$	$0.153 \pm 0.0008$	$0.694 \pm 0.0068$
Rad21-mEos3	$0.001 \pm 0.0001$	n/a	$0.465 \pm 0.0018$

# Supplementary Figure 3

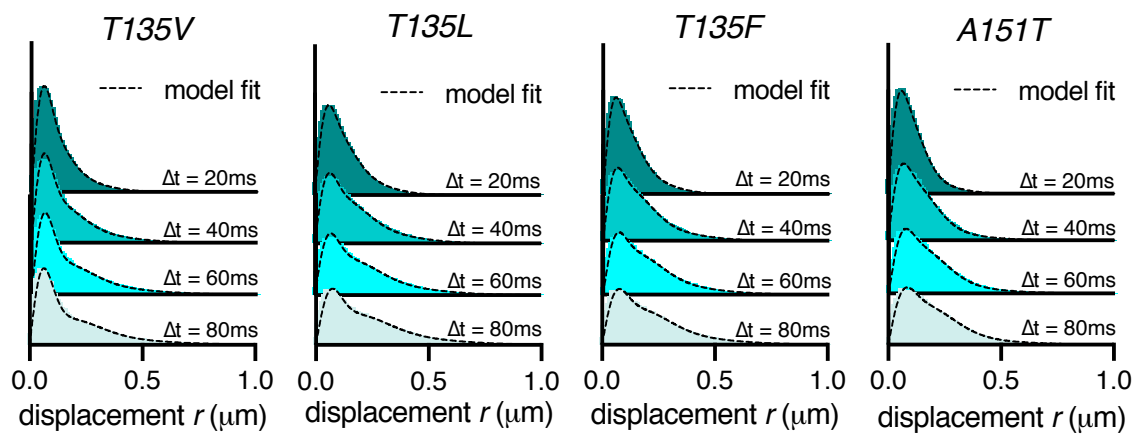
A



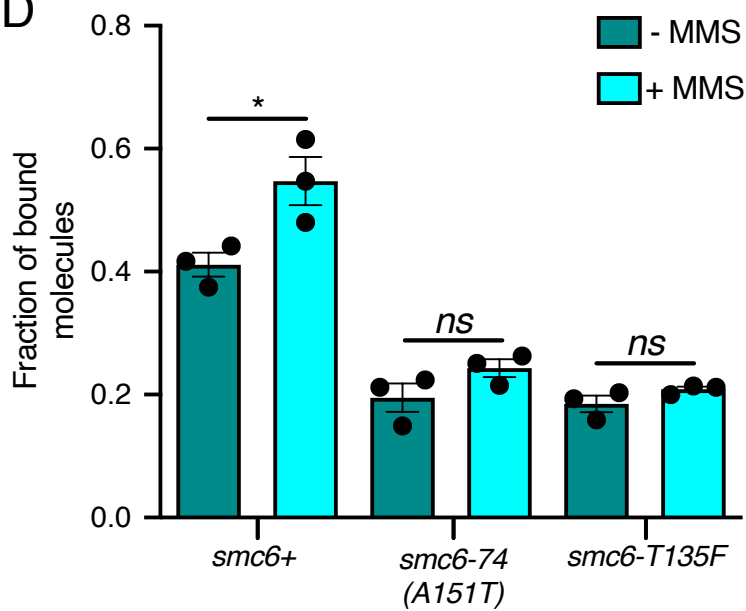
B



C

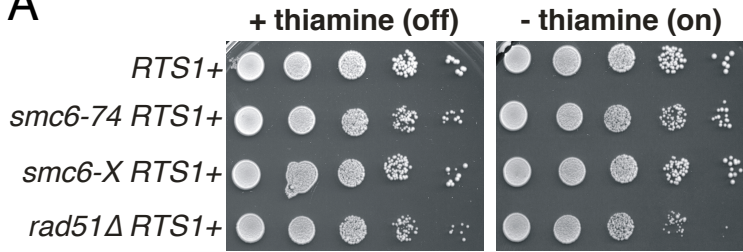


D

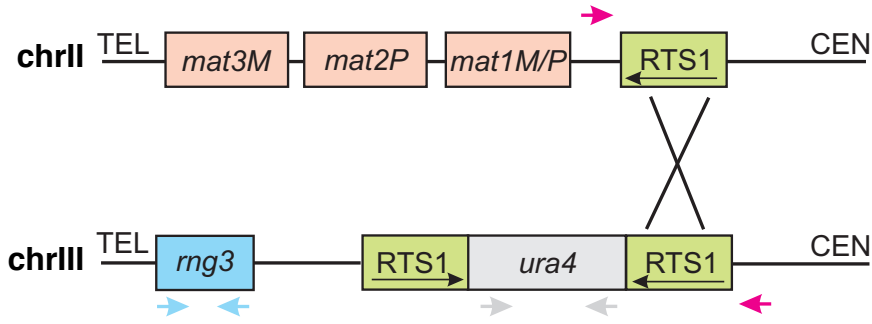


# Supplementary Figure 4

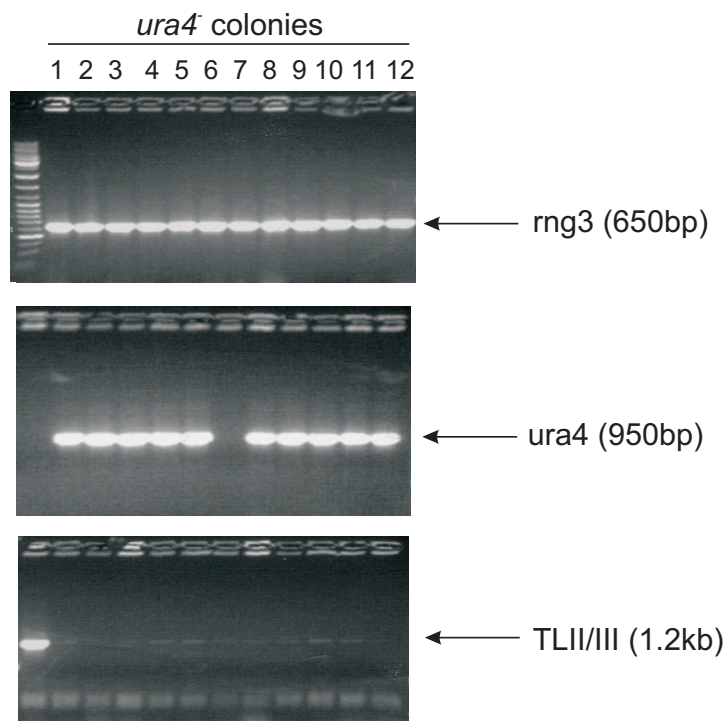
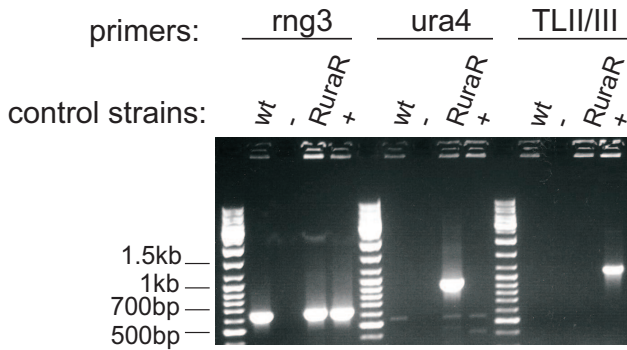
**A**



**B**

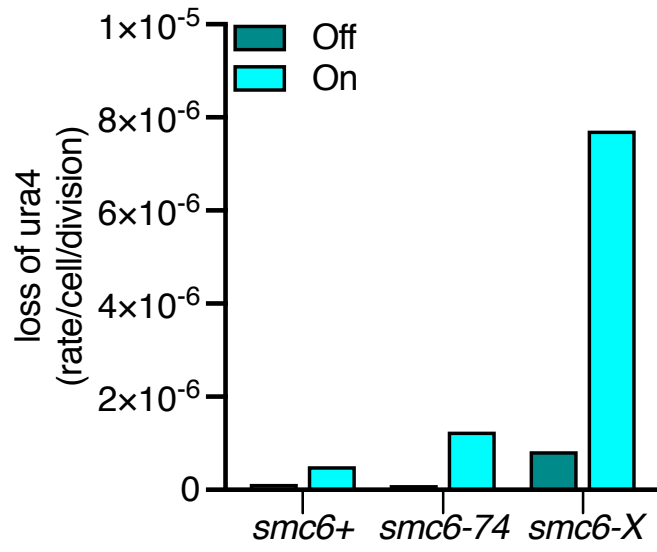


**C**



# Supplementary Figure 5

A



# Supplementary Tables

Table 1

Rate of <i>ura4</i> loss per cell per generation								
Strain	Off (+thiamine)	Relative to <i>smc6</i> <sup>+</sup>	P-value	On (-thiamine)	Relative to Off	P-value	Relative to <i>smc6</i> <sup>+</sup>	P-value
<i>smc6</i> <sup>+</sup>	1.18 x 10 <sup>-7</sup>	1	n.a.	4.39 x 10 <sup>-7</sup>	3.7	0.03	1	n.a.
<i>smc6-74</i>	9.41 x 10 <sup>-8</sup>	0.8	0.23	8.89 x 10 <sup>-7</sup>	9.4	0.02	2	0.101
<i>smc6-X</i>	4.71 x 10 <sup>-7</sup>	4	0.16	4.97 x 10 <sup>-6</sup>	10.5	0.045	11	0.046

Table 2

Strain	Translocations		<i>ura4</i> deletion	<i>ura4</i> point mutation	<i>ura4</i> truncation	<i>ura4</i> deletion	<i>ura4</i> point mutation	<i>ura4</i> truncation
	Off	On	Off			On		
<i>smc6</i> <sup>+</sup>	0/36 (0%)	1/36 (3%)	9/36 (25%)	27/36 (75%)	0/36 (0%)	26/36 (72%)	8/36 (22%)	2/36 (6%)
<i>smc6-74</i>	2/36 (6%)	3/36 (8%)	15/36 (42%)	21/36 (58%)	0/36 (0%)	26/36 (72%)	9/36 (25%)	1/36 (3%)
<i>smc6-X</i>	2/36 (6%)	6/36 (17%)	14/36 (39%)	19/36 (53%)	3/36 (8%)	31/36 (86%)	5/36 (14%)	0/36 (0%)

# Supplementary Tables

Table 3

Strain No.	Genotype	Reference
TJE323	<i>loxP-nse4-mEos3.2-loxM3 ura4-D18 leu1-32 ade6-704</i>	This study
TJE350	<i>loxP-smc6-mEos3.2-loxM3 ura4-D18 leu1-32 ade6-704</i>	This study
TJE496	<i>smc1-loxP-mEos3.2:kanMX6-loxM3 ura4-D18 leu1-32</i>	This study
TJE480	<i>loxP-nse4-mEos3.2-loxM3 loxP-smc6-T135V-loxM3 ura4-D18 leu1-32 ade6-704</i>	This study
TJE477	<i>loxP-nse4-mEos3.2-loxM3 loxP-smc6-T135L-loxM3 ura4-D18 leu1-32 ade6-704</i>	This study
TJE475	<i>loxP-nse4-mEos3.2-loxM3 loxP-smc6-T135F-loxM3 ura4-D18 leu1-32 ade6-704</i>	This study
TJE410	<i>loxP-nse4-mEos3.2-loxM3 smc6-A151T ura4-D18 leu1-32 ade6-704</i>	This study
TJE719	<i>loxP-nse4-mEos3.2-loxM3 loxP-smc6-R150A-loxM3 ura4-D18 leu1-32 ade6-704</i>	This study
TJE711	<i>loxP-nse4-mEos3.2-loxM3 loxP-smc5-R77A-loxM3 ura4-D18 leu1-32 ade6-704</i>	This study
TJE509	<i>loxP-nse4-mEos3.2-loxM3 smc6-F528A ura4-D18 leu1-32 ade6-704</i>	This study
TJE483	<i>loxP-nse4-mEos3.2-loxM3 smc5-R609E R615E ura4-D18 leu1-32 ade6-704</i>	This study
TJE671	<i>loxP-nse4-mEos3.2-loxM3 smc5-Y612G ura4-D18 leu1-32 ade6-704</i>	This study
TJE418	<i>loxP-nse4-mEos3.2-loxM3 smc6-R706C ura4-D18 leu1-32 ade6-704</i>	This study
TJE492	<i>loxP-nse4-mEos3.2-loxM3 loxP-nse3-R254E-loxM3 ura4-D18 leu1-32 ade6-704</i>	This study
TJE730	<i>loxP-nse4-mEos3.2-loxM3 brc1::hphMX6 ura4-D18 leu1-32 ade6-704</i>	This study
TJE734	<i>loxP-nse4-mEos3.2-loxM3 nse6::kanMX6 ura4-D18 leu1-32 ade6-704</i>	This study
TJE796	<i>nse6-loxP-mEos3.2-loxM3 ura4-D18 leu1-32</i>	This study
TJE816	<i>loxP-nse4-mEos3.2-loxM3 hta1-S129A:ura4 hta2-S128A:his3 his3-D1ura4-D18 leu1-32</i>	This study
TJE393	<i>rad21-loxP-mEos3.2:kanMX6-loxM3 ura4-D18 leu1-32</i>	This study
TJE586	<i>nse2-loxP-mEos3.2:kanMX6-loxM3 ura4-D18 leu1-32</i>	This study
TJE522	<i>cnd2-loxP-mEos3.2:kanMX6-loxM3 ura4-D18 leu1-32</i>	This study
HQD87	<i>loxP-smc5+-ura4-loxM3 ura4-D18 leu1-32 ade6-704</i>	This study
DE297	<i>loxP-smc6+-ura4-loxM3 ura4-D18 leu1-32 ade6-704</i>	This study
DE285	<i>loxP-smc6-T135V-loxM3 ura4-D18 leu1-32 ade6-704</i>	This study
DE283	<i>loxP-smc6-T135L-loxM3 ura4-D18 leu1-32 ade6-704</i>	This study
DE281	<i>loxP-smc6-T135F-loxM3 ura4-D18 leu1-32 ade6-704</i>	This study
DE279	<i>loxP-smc6-R150A-loxM3 ura4-D18 leu1-32 ade6-704</i>	This study
DE342	<i>loxP-smc5-R77A-loxM3 ura4-D18 leu1-32 ade6-704</i>	This study
DE273	<i>smc6-A151T ura4-D18 leu1-32 ade6-704</i>	Lab strain
JMM1188	<i>ura4-D18 leu1-32 ade6-704</i>	Lab strain
JMM1162	<i>nmt41:rtf1:sup35 RTS1-ura4-RTS1 ade6-704 leu1-32</i>	Lambert et al 2005
JMM1171	<i>rhp51::NAT nmt41:rtf1:sup35 RTS1-ura4-RTS1 ade6-704 leu1-32</i>	Lambert et al 2005
JMM1371	<i>smc6-A151T nmt41:rtf1:sup35 RTS1-ura4-RTS1 ade6-704 leu1-32</i>	This study
JMM1375	<i>smc6-R706C nmt41:rtf1:sup35 RTS1-ura4-RTS1 ade6-704 leu1-32</i>	This study